EartArXiv Coversheet

Dienes, B.[1], Mendoza, O.[1,2], Bright, K.[1], Licini, G.[1], Aeppli, M.[1,*]

[1]Soil Biogeochemistry laboratory (SOIL), Swiss Federal Institute of Technology Lausanne (EPFL), Sion, Switzerland

[2]Institute of Earth Surface Dynamics, Faculty of Geosciences and the Environment, University of Lausanne, Lausanne, Switzerland

Interactive effects of landscape position and soil diversity drive the spatial variability of soil organic carbon concentration in subalpine soils of Switzerland

Dienes, B.[1], Mendoza, O.[1,2], Bright, K.[1], Licini, G.[1], Aeppli, M.[1,*]

[1]Soil Biogeochemistry laboratory (SOIL), Swiss Federal Institute of Technology Lausanne (EPFL), Sion, Switzerland

[2]Institute of Earth Surface Dynamics, Faculty of Geosciences and the Environment, University of Lausanne, Lausanne, Switzerland

[*] correspondence: meret.aeppli@epfl.ch, +41 21 693 72 79

Abstract: Subalpine soils store a significant amount of soil organic carbon (SOC), yet the factors driving its landscape-scale variability remain poorly constrained. Although topography, soil type, soil texture, and moisture are recognised as key drivers of SOC concentration, their interactive effects in subalpine environments remain largely unexplored. In particular, the extent to which soil type shapes landscape-scale SOC patterns remains unclear. In this study, we assessed SOC concentration, soil type, soil moisture conditions and texture, elemental composition across 100 plots in two subalpine catchments in the Swiss Alps. Using factor analysis, we generated three standardised continuous predictors from our dataset, namely, mineral content, sedimentary rock influence and texture index. We investigated the joint influence of these continuous predictors on SOC variability at the landscape scale in a linear mixed-effects model with topography (plain vs. slope areas), soil depth and soil type as additional categorical predictors. We found that soil type diversity was greater on the plain than on the slope, reflecting a greater hydrological heterogeneity. Plains supported a broad spectrum of soils, ranging from organic-rich Histosols to mineral-rich Fluvisols, while slopes were dominated by Cambisols. Although plains exhibited higher moisture and SOC concentration, and slopes were characterised by higher clay fractions and lithogenous elements, topographic position alone was insufficient to explain the

observed spatial distribution of SOC. Our linear mixed-effect model identified mineral content as the strongest predictor of SOC concentration, followed by sedimentary rock influence and the texture index. SOC concentration decreased as mineral content and sedimentary rock influence increased, and as the texture index shifted towards a higher proportion of clay-sized particles. Crucially, while mineral content integrates much of the variability described by the categorical variables included in the model, soil type diversity effectively captures the range of mineral content that drives SOC concentration across our sampling locations and soil depth. Our findings suggest that relying strictly on topographic positions overlooks important nuances in soil property distribution and SOC concentration. We therefore suggest that soil type provides a more integrative predictor of landscape-scale SOC variability in subalpine environments than topographic position alone.

Keywords: Soil organic carbon, subalpine, soil type, spatial variability, topography, soil texture

1 Introduction

Alpine and subalpine soils are rich in soil organic carbon (SOC) and store a disproportionate share of SOC relative to their small spatial area (Körner, 2021). At the landscape scale, SOC variability is pronounced because spatially variable soil-forming factors, such as topography, parent material and pedoclimate, create a high diversity of soil types (Poulenard and Podwojewski, 2005). Topography, soil moisture, soil texture, and soil type have been identified as key drivers of SOC content across environments and spatial scales (Arrouays et al., 2001; Bai and Zhou, 2020; Wiesmeier et al., 2014). However, in subalpine environments, studies report contrasting effects of topography and soil texture on landscape-scale SOC patterns (Ferré et al., 2020; Hoffmann et al., 2014; Luo et al., 2024), and their interactive influence with soil moisture and soil type on SOC variability remains poorly constrained.

Topography is a primary soil-forming factor and is especially influential in alpine landscapes because it structures the spatial variability of other soil-forming factors (Birkeland, 1999). By governing erosion, deposition, and transport, topography shapes the distribution of parent material across the landscape. It also regulates pedoclimate through exposure, aspect, and critically through hydrological flow paths, which in turn affect soil moisture patterns. Through these properties, it exerts strong control on landscape-scale SOC patterns because moisture and aeration directly regulate SOC accumulation and mineralization. In plain and low topographic positions, SOC can accumulate when waterlogging limits oxygen supply and inhibits mineralization (Dickopp et al., 2018). Accordingly, terrain-derived metrics, such as topographic position and the topographic wetness index, have been used successfully to predict SOC content (Patton et al., 2019; Wiesmeier et al., 2014; Zhu et al., 2019). Reported SOC patterns across topographic positions in subalpine environments remain inconsistent; previous studies have variously documented higher SOC content on the slope (Ferré et al., 2020), on the plain (Luo et al., 2024) or no significant spatial pattern (Garcia-Pausas et al., 2007; Hoffmann et al., 2014). However, these studies have not thoroughly investigated the confounding effect of soil moisture.

In addition to soil moisture, topography also structures landscape-scale variation in soil texture by governing the distribution and weathering of parent material in subalpine terrain (Poulenard and Podwojewski, 2005). As mineral substrates weather, pedogenic minerals form and increase

the clay-sized fraction, leading to finer textures. These pedogenic minerals are central to SOC stabilization through organo-mineral interactions (Kleber et al., 2015). Across many ecosystems, SOC content increases with the proportion of fine particles, yet this relationship is less consistent in subalpine soils (Ferré et al., 2020; Garcia-Pausas et al., 2007; Hoffmann et al., 2014; Luo et al., 2024). One likely reason is that texture effects are not independent: their influence on SOC may be contingent on hydrological setting and topographic position, which regulate saturation, redox conditions, and mineral reactivity. However, studies that explicitly test these interactive effects are limited (Françoys et al., 2024), and none, to our knowledge, have been conducted in subalpine soils.

Soil type integrates multiple controls on SOC concentration because it reflects the combined influence of topography, parent material, and microclimate on soil properties that govern SOC stabilization and accumulation (Kögel-Knabner and Amelung, 2021; Matteodo et al., 2018). Accordingly, soil type is an important predictor of SOC content at regional scales (Arrouays et al., 2001; Bell and Worrall, 2009), and its relevance for (sub)alpine regions has been demonstrated even where spatial variability is represented only coarsely (Wiesmeier et al., 2014). In subalpine environments, the extent to which soil type variability drives landscape-scale SOC variability remains poorly constrained.

Here, we assess how topography, soil moisture, soil texture, and soil type jointly control landscape-scale variability in SOC concentration across heterogeneous subalpine catchments. We selected 100 plots in two subalpine sites in the Swiss Alps, spanning two contrasted topographic positions, namely plain and slope, comprising several soil types, and a range of soil physicochemical properties and soil moisture conditions. We sampled up to three soil depth ranges, namely 0-10 cm, 10-30 cm and 30-50 cm, quantified elemental composition, soil texture, and soil pH. Soil moisture and temperature were monitored for a year at depths of 10 and 30 cm across 24 locations. The specific objectives of this study were (1) to assess the effect of contrasted subalpine topographic position on SOC concentration, selected soil properties and soil types; and (2) to identify the drivers of spatial variability in SOC concentration at the landscape scale. We hypothesised that (1) SOC concentration is higher and more variable on the plain than on the slope, reflecting variations mainly in soil moisture and soil type; (2) the variability of soil type

drives the spatial variability in SOC concentration at the landscape scale, particularly on the plain, where soil moisture conditions and soil formation are more diverse than on the slope.

2 Methods

2.1 Study site

We selected two study sites in the central Swiss Alps: Blatt in the Binntal (∼2100 m.a.s.l., 46°22'N/8°16'E; Figure 1, top-right) with a mean annual temperature of 1.3 °C and 1834 mm of mean annual precipitation (data extrapolated from the nearest station, Grimsel Hospiz, 1980 m a.b.sl., 21 km from the study area; www.meteosuisse.ch), and Ar du Tsan in the Vallon de Réchy (∼2200 m.a.s.l., 46°12'N/7°30'E; Figure 1, bottom-left) with a mean annual temperature of 1.9 °C and a mean annual precipitation of 1000 mm (data extrapolated from the nearest station, Evolène, 1825 m.a.s.l., 8 km from the study site; www.meteosuisse.ch). Each site is characterised by two major topographical entities: a large hillslope descending to a vast plain. The slope in Blatt has an S aspect and runs for about 220 meters at a 30° angle. The slope in Ar du Tsan has an E aspect and is slightly shorter and less steep, with 180 meters and a 26° angle. The slope and the plain are described as an undifferentiated moraine and mixed alluvium, respectively. Both of these detritic materials originated from gneiss belonging to the Monte Leone geological unit in Blatt and the Siviez-Mischabel one in Ar du Tsan (Carrupt, 2003; Marthaler et al., 2008) and, sedimentary rocks, specifically dolomite, gypsum, calcschist and cornieul, from the Tsaté and Cimes Blanches Units in Ar du Tsan and the Mt Leone and Camosci Units in Blatt (Carrupt, 2003; Marthaler et al., 2008). In both sites, the vegetation on the slope is dominated by a mixture of subalpine acidophilous grassland and heaths (Freléchoux and Gallandat, 1995; Richard et al., 1993, Figure S1 and S2), reflecting a xeric environment. Naturally, the water flows from the slope by surface run-off or in one or two more pronounced seepages towards the plain, which is crossed by diffuse channels, converging to a watercourse. In Ar du Tsan, la Rèche runs along the east limit of the study site, and in Blatt, die Binna marks the southern limit of the study site. On the plains, the vegetation reflects the wet to water-logged situation prevailing there, with plant community types typical of alkaline and acidophilic fens (Freléchoux

and Gallandat, 1995; Richard et al., 1993, Figure S1 and S2).

2.2 Soil type assessment and mapping

The soil types of the two catchments were assessed through soil pits and auger cores. In total, 18 soil pits were described and classified in the field using the Référentiel pédologique (Baize and Girard, 2008) and then translated into the World Reference Base classification system (WRB) (WRB, 2022). We linked these soil types to standalone reference soil groups of the WRB and added a qualifier when necessary to nuance between reference soil groups. These names were used throughout the text. To map the soil types of each study site, we used the spatial information from the pits, auger cores and additional soil surveys (Figure S3) and established the limits of each soil type based on this information and clear topographic ruptures. The map was used to attribute a soil type to each plot.

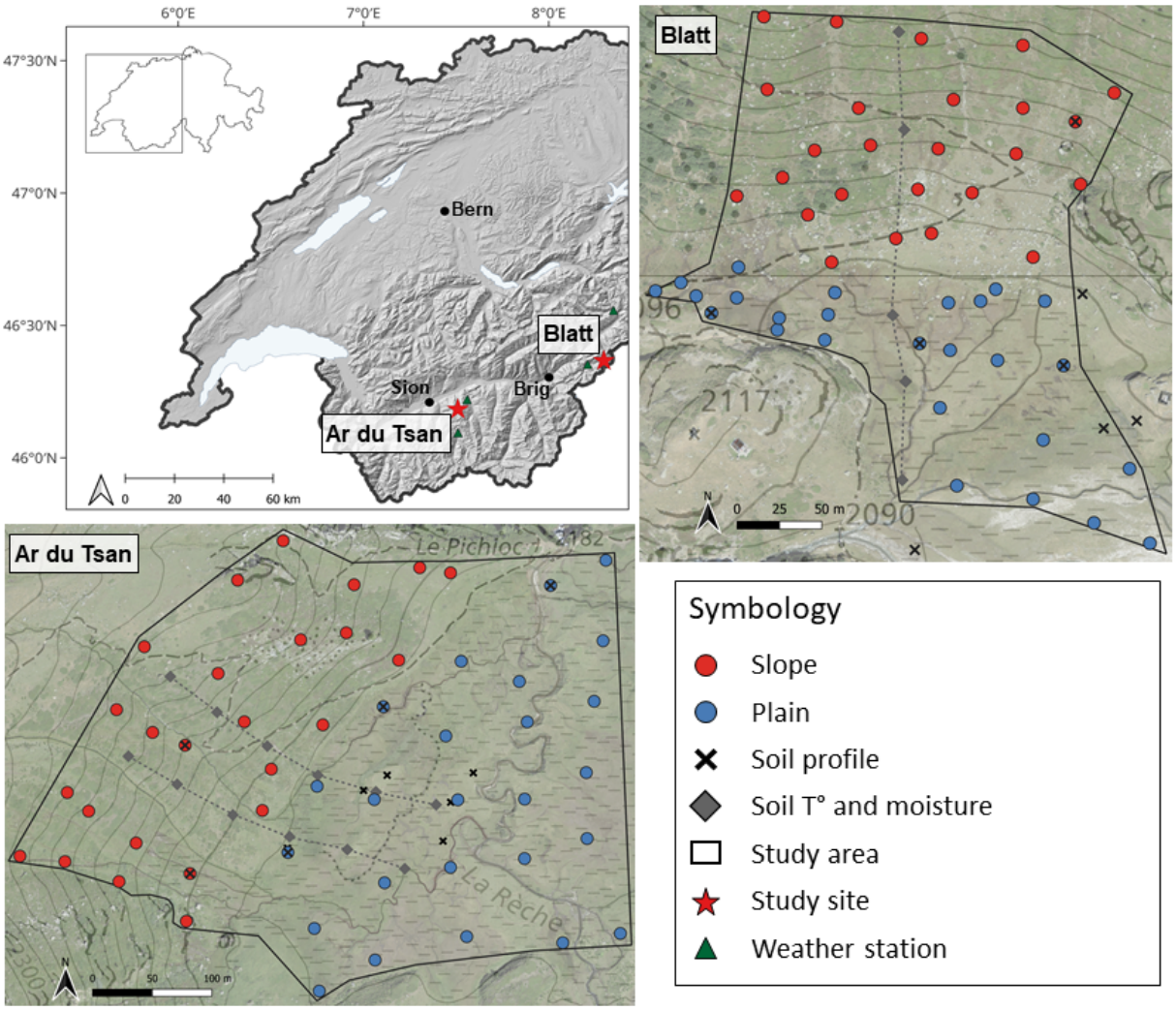

Figure 1: Location of study sites and sampling plots. Each study site has 25 plots on the slope (red dots) and 25 plots on the plain (blue dots), for a total of 100 plots. Four soil profiles (black cross) were characterised on the slope and 14 on the plain.

2.3 Soil temperature and moisture monitoring

Soil temperature and volumetric soil moisture content (θ_v) were monitored at 15-minute intervals for one year (September 2023 - August 2024) along transects spanning each site from the upper slope to the distal plain (Figure 1). Six measurement locations were spanned along each transect. Each measurement location consisted of two TOMST loggers (TMS dataloggers, TOMST®, Czech Republic), a TMS Standard and a TMS Burial buried horizontally at 10 and 30 cm depth, respectively. Soil disturbance was kept to a minimum during installation, and care was taken to ensure good contact between the soil and the moisture measurement blade. The

temperature values represent the average of three measurements at 10 cm and two measurements at 30 cm. Volumetric water content (m^3 m^{-3}) was calculated from the raw moisture counts using the myClim package (Man et al., 2023) on R. Within the package, several pre-calibrated soil types are available to account for differences in soil properties. We used the peat soil type (Wild et al., 2019) when soils were very organic and the universal soil type (Kopecký et al., 2021) in all other cases.

2.4 Soil sampling and preparation

We applied a grid sampling approach at both sampling sites with an equal number of 25 plots each for the slope and the plain (Figure 1). In summer 2023, 100 plots were sampled at a maximum of three depth ranges (0-10 cm, 10-30 cm and 30-50 cm) where the soil was deep enough, for a total of 253 samples (0-10 cm: 101 samples, 10-30 cm: 88 samples, and 30-50 cm: 64 samples). Samples were taken from a recomposed soil core excavated with an auger. The samples were stored in ziplock bags, transported to the laboratory in a cool bag, and immediately air-dried upon return from the field site, except for a small aliquot reserved for pH, hygroscopic moisture content (HMC) and loss on ignition (LOI) measurements. The remaining bulk sample was air-dried and sieved at 2 mm before collecting another aliquot that was crushed with a planetary micro mill (Pulverisette 7, Fritsch, Germany).

2.5 Soil analysis

Soil pH was measured on fresh soil in deionised water with a 1:5 soil:solution ratio after 30 minutes of agitation at 200 RPM and 30 minutes settling time with a pH meter (SevenDirect SD50, Mettler Toledo, Switzerland). We used approximately 2 g of air-dried soil to assess HMC and LOI. HMC was assessed as the mass difference between air-dried soil and oven-dried soil at 105 °C for 16 hours, and LOI was assessed using the mass difference between air-dried soil and combusted soil at 450 °C for 16 hours. HMC was used as a mass correction factor to report all mass-dependent analyses as dry soil weight. Soil texture was analysed with a grain sizer using laser diffraction (LS 13 320, Beckman Coulter, Germany) on 0.5 g of air-dried and sieved soil after digestion of organic matter with hydrogen peroxide for approximately 2 weeks. The

readings were pooled together in three size fractions [%v v^{-1}] as follows: sand (2000 µm - 50 µm), silt (50 µm - 2 µm) and clay (≤2 µm). Carbon and nitrogen concentrations were measured by chromatography after combustion at 900 °C of 10 mg of crushed soil on a CHNS element analyser (Flash EA 1112, Thermo Finnigan, US). When mineral contribution to total C concentration was suspected, samples were fumigated with 37% HCl for 16 hours to remove all carbonates. Mineral contribution to total N concentration is negligible. Therefore, C and N concentrations were assumed to represent soil organic carbon and total nitrogen (TN), respectively. Elemental composition of Al, Ca, Cl, Fe, K, Mg, Mn, Na, P, S and Si was measured on 5 g of crushed soil with a benchtop XRF (Xepo5, Spectro Xepos, Germany). Element concentrations are expressed as mass fractions relative to the mass of dry soil.

2.6 Statistical analysis

Differences in SOC, N, carbon-to-nitrogen (CN) ratio, soil pH, soil texture, and total elemental concentrations were tested among topographic positions (plain vs. slope) using Yuen's trimmed mean test, and among soil depths (0-10 cm, 10-30 cm and 30-50 cm) within each topographic position using a one-way ANOVA on trimmed means (Wilcox, 2022). Differences between study sites were also evaluated using the same tests to assess potential site-level variation to account for in subsequent analyses.

Soil pH, CN ratio, soil texture and total elemental concentration were combined in a principal factor analysis to account for correlation among variables and differences in units and magnitudes. Three factors were computed using a factor analysis with minimum residues (minres) as the factoring method and an oblique rotation (promax). Factors were assigned ecological meaning based on the loadings of soil properties. Only loadings with absolute values ≥ 0.5 were selected, and higher loadings contributed more strongly to interpretation. Factor scores for each observation were used as predictors in the mixed-effects models described below.

The relationship between SOC and soil properties, expressed as factors, was investigated using linear mixed-effect modelling. The fixed effects included the three factors from the preceding factor analysis, namely mineral content, texture index and sedimentary rock influence as continuous standardised predictors, and topographic position, study site, soil depth and soil type as

categorical predictors. Plot was included as a random grouping factor, with an autoregressive correlation structure (AR1) to account for repeated measurements. Marginal and conditional R^2 were computed following Nakagawa and Schielzeth (2013). The residual variance was approximated using the base variance parameter of the linear mixed-effects model. Model assumptions, including normality of residuals and homoscedasticity, were evaluated visually with Q-Q plots and residuals vs. fitted values. All analyses were conducted in R using the following packages: nlme (Pinheiro et al., 2025) for linear mixed-effect modelling, psych (William Revelle, 2025) for factor analysis and WSR2 (Mair and Wilcox, 2014) for analysis of variance.

3 Results

3.1 Soil moisture and soil types across topographic positions

The mean annual volumetric soil moisture content (θ_v) at 10 cm soil depth over the measurement period was 0.9 m^3 m^{-3} in Blatt and 0.7 m^3 m^{-3} in Ar du Tsan (Table 1). At 30 cm depth, this value increased to 1.0 m^3 m^{-3} in Blatt but remained constant at 0.7 m^3 m^{-3} in Ar du Tsan (Table S1). The variability of θ_v at 10 cm depth among the measurement points on the plain was lower in Blatt (0.7 - 1.0 m^3 m^{-3}) than in Ar du Tsan (0.3 - 1.0 m^3 m^{-3}) (Table S1). The variability in soil moisture conditions was also evidenced by the variety of plant community types, ranging from associations characteristic of grassland to wetland associations, with the latter dominating on both plains (Table 1).

The mean annual θ_v was lower on the slope than on the plain and constant over the two monitored soil depths (0.4 m^3 m^{-3} for both catchments, Table S1). θ_v variability at 10 cm depth was lower in Blatt (0.4 - 0.5 m^3 m^{-3}) compared to Ar du Tsan (0.3 - 0.5 m^3 m^{-3}) (Table 1). However, unmonitored wetter locations linked to local oozings were observed in both catchments. The dominant plant community types reported on both slopes were alternating heath and grassland plant community types (Table 1). Plant community types of wet environments, such as oozings, and linked to cattleing and more eutrophic environments, were locally reported on the slope (Freléchoux and Gallandat, 1995; Richard et al., 1993).

The assessment of soil profiles revealed greater diversity of soil types on the plain than on

Table 1: Summary table for both study sites of soil moisture and temperature at depths of 10 and 30 cm, habitats, plant community types, soil types following the WRB reference soil groups and lithology.

Study site	Blatt		Ar du Tsan	
Topography	Plain	Slope	Plain	Slope
Soil moisture 10 cm [m^3 m^{-3}]	0.92	0.42	0.68	0.39
Soil moisture 30 cm [m^3 m^{-3}]	0.99	0.38	0.68	0.38
Soil temperature 10 cm [°C]	5.19	5.38	5.05	6.04
Soil temperature 30 cm [°C]	4.99	5.12	4.92	5.98
Habitat	Fen	(sub)alpine grassland, Heath	Fen	(sub)alpine grassland, Heath
Plant community type*	Caricion atrof.-saxatilis, C. davallianae, C. fuscae, Nardion, Poion alpinae	Nardion, Rhododendron-Vaccinion, Caricion davallianae	Calthion, Caricetum rostratae, C. davallianae, C. fuscae, Nardion	Nardion, Caricion fuscae, Rumicion alpini, Cicerbito alpinae-Adenostyletum, Junipero-Arctostyphyletum, Loiseleurio-Vaccinion, Cratoneuretum falcati
Reference soil groups (WRB)	Fluvisols, Histic Leptosols, Histosols, Epileptic Histosols, Regosols	Cambisols, Histic Leptosols, Regosols	Fluvisols, Histic Leptosols, Histosols, Epileptic Histosols, Podzols, Regosols	Cambisols, Histic Leptosols
Lithology	mixed alluvium	mixed moraine	mixed alluvium	mixed moraine

Note: Soil temperature and moisture values are yearly averages 2023-2024. Detailed temporal trends can be found at alpinesoc.epfl.ch
* From Freléchoux and Gallandat (1995) and Richard et al. (1993), with the addition of oozing vegetation.
** As described in Swisstopo.

the slope (Figure 2). On the plain, we observed a gradient of soil types ranging from well-developed Histosols with thick histic layers (>2 m deep) to Fluviosols with little organic material accumulation. Epileptic Histosols (Fluvic), Histic Leptosols, Regosols, and Podzols were typical of intermediate locations. Epileptic Histosols (Fluvic) had a thin histic layer (<50 cm) over fine material deposited on the moraine. Histic Leptosols displayed a fine histic layer (<15 cm) directly on morainic material. Their spatial distribution was linked to their distance from the main stream (Figure 2). Regosols appeared locally on small bumps or at the periphery of the study site. Podzols were confined to Ar du Tsan's plain and were found in a restricted area on an inactive dejection cone at the bottom of the slope and covered with *Calthion* as the plant community type. Leptic Cambisol (Colluvic) dominated the slopes, while Histic Leptosols appeared only locally in connection with oozings. A description of the soil profiles is provided in the Supplementary Information (Figures S4).

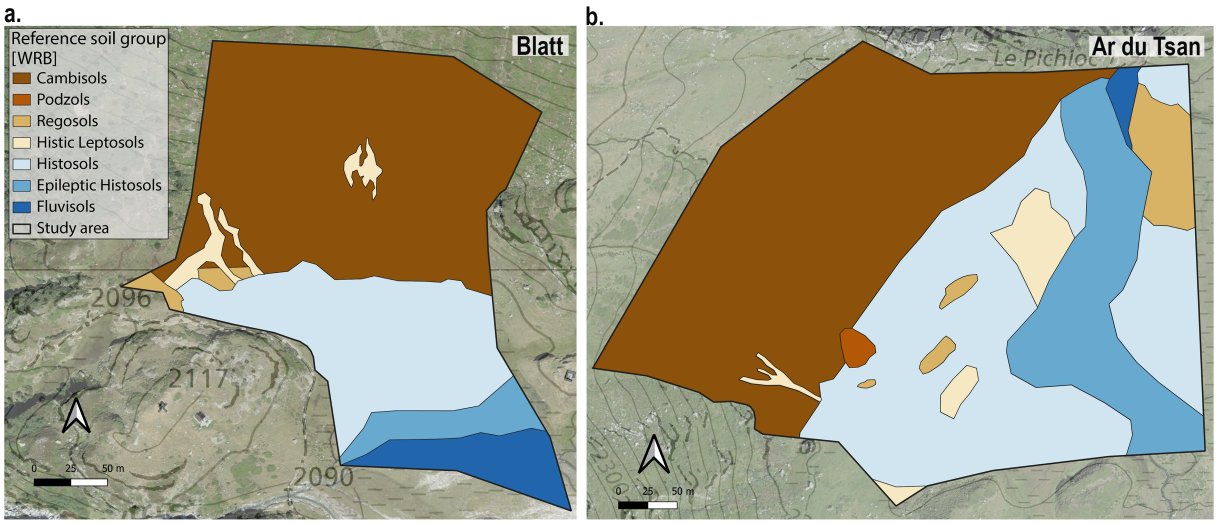

Figure 2: Spatial distribution of Reference soil groups (WRB) within the study area. Panels show soil group maps for **a.** Blatt and **b.** Ar du Tsan, overlaid on an orthophoto and a topographic (1:25'000) basemap from Swisstopo. Reference soil groups include Cambisols, Podzols, Regosols, Leptosols, Histosols, Epileptic Histosols, and Fluvisols. The black outline indicates the study area boundary.

3.2 Soil physicochemical properties across topographic positions

We found significantly higher SOC concentrations on the plain (19.93 ± 16.82%) than on the slope (6.39 ± 5.77%, p <.001, Figure 3a). SOC concentrations were constant across soil depth

on the plain but decreased with soil depth on the slope, from 9.68 ± 6.28% at 0-10 cm, to 1.96 ± 0.67% at 30-50 cm ($p < .001$, Figure 3a). TN concentrations followed a similar pattern to SOC (Figure S5a); however, the CN ratio was significantly higher on the plain, 19.73 ± 6.31, compared to the slope, 14.95 ± 3.51 ($p < .001$, Figure S5b).

Topography also influenced soil texture, mineral composition, and pH. Among the three texture classes, only clay was significantly higher on the slope (4.35 ± 1.86% v v^{-1}) than on the plain (2.57 ± 1.4% v v^{-1}, $p < .001$) (Figure 3b), while silt ($p = 0.59$, Figure 3c) and sand content did not differ between topographic positions (Figure S5c). This topographic effect was also reflected in the mineral concentration profiles (Figure 3d-h). The slope had higher concentrations of Al, Fe and Si than the plain (Al: 73.36 ± 12.64 mg g^{-1} vs. 55.39 ± 31.01 mg g^{-1}, $p < .001$; Fe: 31.35 ± 10.91 mg g^{-1} vs. 21.04 ± 13.17 mg g^{-1}, $p < .001$; Si: 301.81 ± 42.83 mg g^{-1} vs. 190.85 ± 110.37 mg g^{-1}, $p = 0.03$). On the slope, Al and Si concentrations were significantly higher at 10-50 cm than at 0-10 cm (all $p<.001$). K ($p<.001$), Mn ($p<.001$), Na ($p<.001$) and P ($p = 0.007$) concentrations were also significantly higher on the slope than on the plain (Figure S5d-f:h). Conversely, Ca concentrations were higher on the plain, 14.50 ± 17.12 mg g^{-1}, than on the slope, 7.14 ± 3.75 mg g^{-1} ($p < .001$), while Mg concentrations did not vary between the two topographic positions ($p = 0.49$). The plain had higher Cl ($p<.001$) and S ($p<.001$) concentrations than the slope (Figure S5g:i). Soil pH was slightly higher on the plain, 5.94 ± 0.93, than on the slope, 5.49 ± 0.6 ($p < .001$, Figure 3i).

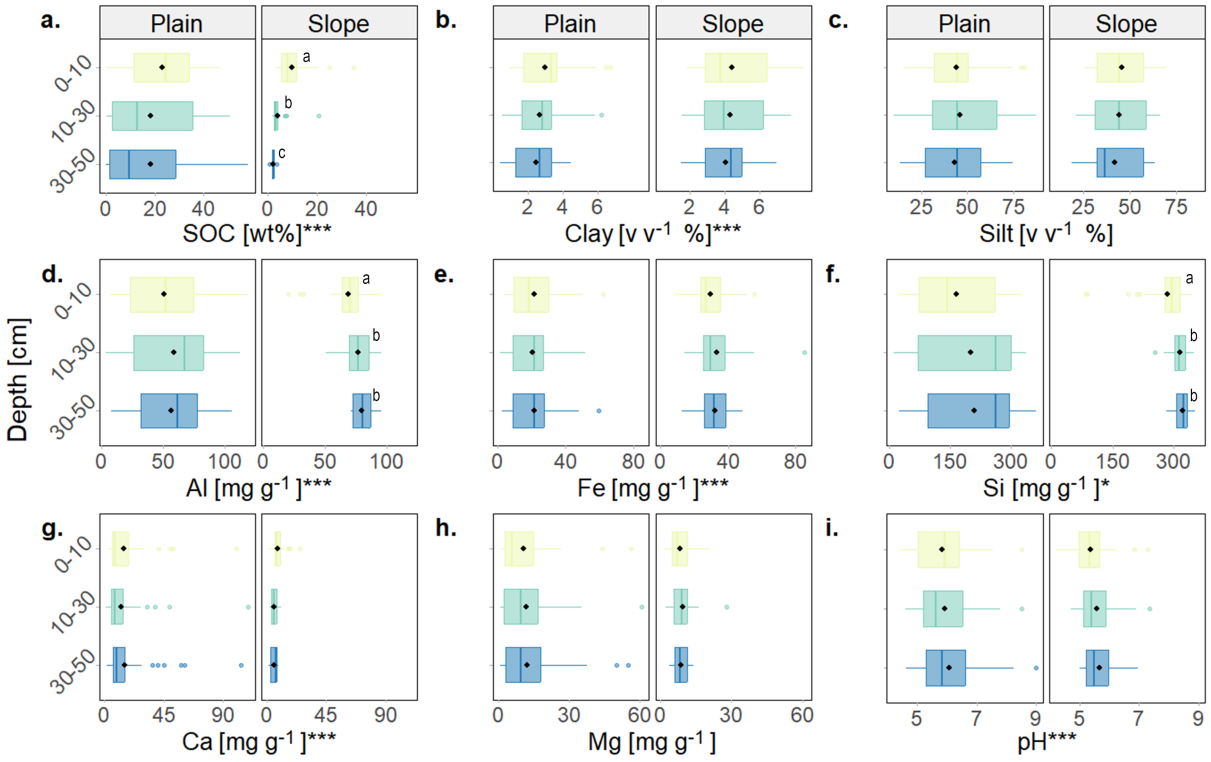

Figure 3: Depth profiles of soil physicochemical properties in plain and slope positions. Concentrations of **a.** Soil organic carbon (SOC). **b.** Clay. **c.** Silt. **d.** Aluminium (Al). **e.** Iron (Fe). **f.** Silicium (Si). **g.** Calcium (Ca). **h.** Magnesium (Mg). **i.** Soil pH. Limits of the box represent the interquartile range. The edges of the left and right whiskers represent the first and fourth quartiles, respectively. Outliers are shown by dots. The median is represented by the black line. Black diamonds represent the box's mean. Significant differences between topographic positions are indicated by asterisks as follows <0.05(*), <0.01(**) and <0.001(***). Lowercase letters indicate significant differences among depths within the same topographic position.

3.3 Drivers of soil organic carbon concentration at the landscape scale

We used principal factor analysis to identify the three main factors driving soil organic carbon concentration based on the soil physicochemical data: mineral content, texture index, and sedimentary rock influence (Figure 4a). Mineral content had high positive loadings of Si (0.93), K (0.86), and Al (0.85), with additional positive loadings of Na (0.74), Fe (0.67), and Mn (0.55) and negative loadings of S (-0.7) and the CN ratio (-0.52). It therefore represents a gradient from mineral-rich soils (positive) to organic matter-rich soils (negative). The texture index had strong positive loadings of silt (0.96) and clay (0.76), and a strong negative loading of sand (-1), representing a gradient from fine- (positive) to coarse-textured (negative) soils. Sedimentary

rock influence had strong positive loadings of Mg (0.87), Ca (0.76) and pH (0.72), reflecting soils influenced by carbonate-rich sedimentary rocks; higher factor values corresponded to higher Mg and Ca content, and pH. Taken together, these three factors captured 64% of the common variance in the dataset, with mineral content explaining 30%, texture index 20%, and sedimentary rock influence 14%.

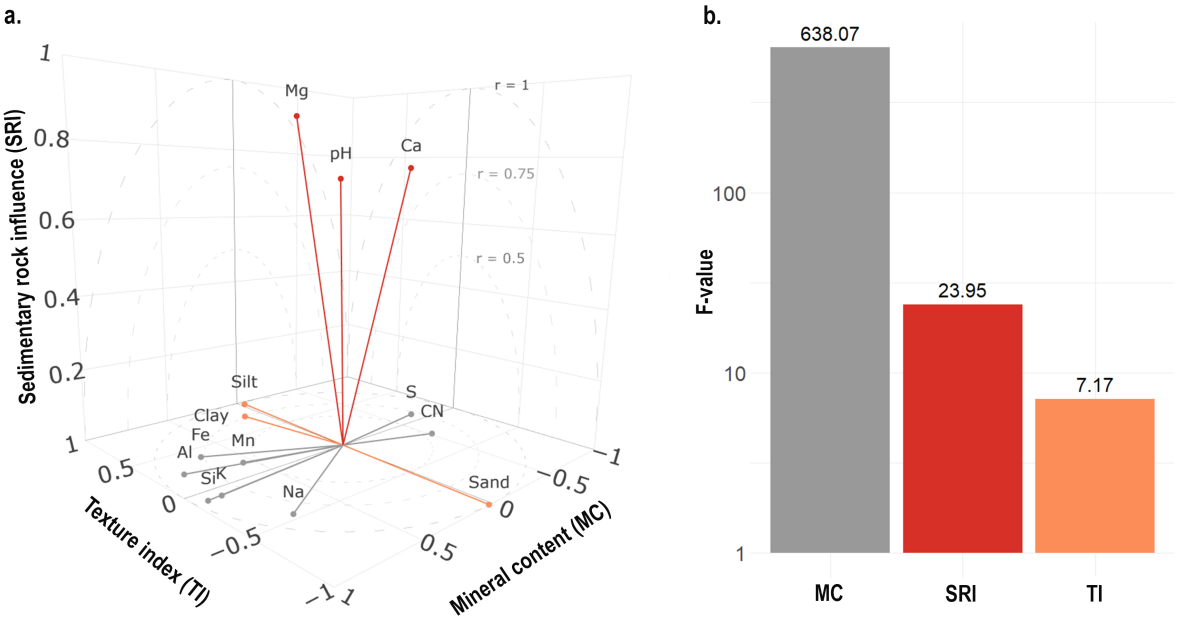

Figure 4: Analysis of factors driving soil organic carbon concentrations. **a.** Relationships between soil physicochemical variables and the three factors, namely mineral content, texture index, and sedimentary rock influence. Vectors indicate the direction and strength of correlations of individual variables with the ordination axes (loadings). Variables with loadings <0.5 were discarded. Along the Z-axis, loadings <0.5 were set to zero. **b.** Relative importance of the three identified factors expressed as F-values on a log-scale, highlighting the dominant influence of mineral content compared to sedimentary rock influence and texture index. Full loadings for all variables and the model's summary table are provided in the Supplementary Information (Table S2 and S3).

Fixed effects explained most variation in SOC concentration (R^2 marginal = 0.93). The majority of the between-plot variability, accounted for with the random effect, was already captured by fixed effects ($\Delta R^2 = 0.007$), and the residual variance from the model is low (~13%). F-values from the model were used to compare the relative contributions of the predictors (Figure 4b). Among the soil property factors, mineral content had the largest F-value (F = 638.07, p <.001), followed by sedimentary rock influence (F = 23.95, p <.001), and soil texture index (F = 7.17, p = 0.008). SOC concentration increased with decreasing mineral content values, decreased with

increasing sedimentary rock influence values, and decreased with higher texture index values (Table S3). Among the categorical fixed effects, topographic position ($F = 4.58$, $p = 0.03$), soil depth ($F = 4.96$, $p = 0.008$), and soil type ($F = 2.75$, $p = 0.02$) had significant effects on SOC concentration, whereas the effect of the study site was not significant ($F = 0.48$, $p = 0.48$). The model indicates that SOC concentration decreased on the slope and with soil depth (Table S3).

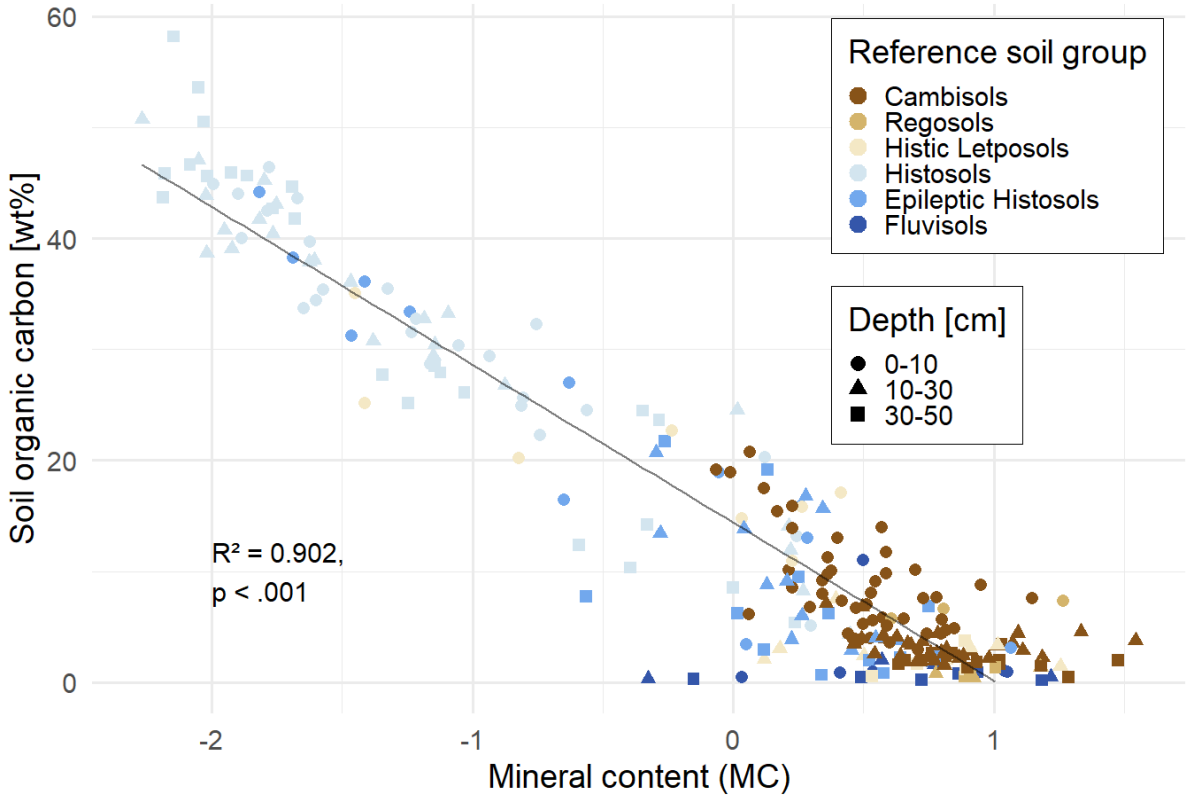

Figure 5: Relationship between mineral content and soil organic carbon concentration across the study areas. Points are colored by Reference soil groups (WRB), and symbols refer to soil depth (0–10: circle, 10–30: triangle, and 30–50 cm: square). The solid line represents the fitted linear regression, indicating a strong negative relationship between mineral content and SOC ($R^2 = 0.90$, $p < .001$).

Mineral content explained most of the variability in SOC concentration, as evidenced from the high F-value ($F = 638.07$, $p < .001$, Figure 4b) and the strong linear relationship between SOC concentration and mineral content ($R^2 = 0.90$, $p < .001$, Figure 5). Figure 5 also shows the distribution of reference soil groups along the gradient in mineral content, with histic layers generally having mineral content <0 and relatively high SOC concentrations, and other soil layers having mineral content >0 and relatively low SOC concentration.

4 Discussion

4.1 Topography and hydrology drive higher soil-type variability on plains than on slopes

Our observations reveal that topographic position, soil moisture content and hydrological processes strongly influenced soil formation in our study sites (Figure 6). On the plains, waterlogged conditions coincided with the presence of histic layers and fen type plant communities. The thickness of the histic layers varied dramatically across both plains: it was thinner near the river and increased toward the slope, where thick histic deposits (>2m, Figure S4) indicate a long history of waterlogged conditions. This variation largely reflected the proximity of the parent material to the soil surface, which was the criterion used to distinguish between Histosols, Epileptic Histosols, and Histic Leptosols. Sampling plots closest to the river, particularly in Blatt, were dominated by Fluvisols, as sediment transport was too strong for a histic layer to develop. In Blatt, the river margins showed repeated sequences of Fluvisols, consistent with frequent flooding and associated with a distinct plant community types (*Caricion bicoloir-atrofuscae*, Freléchoux and Gallandat, 1995). On the plain, lower volumetric soil moisture content coincided with Regosols and *Nardion* in both catchments and, in Ar du Tsan, also Podzols and *Calthion* (Freléchoux and Gallandat, 1995; Richard et al., 1993).

On the slopes, most soils were shallow and well-drained and affected by colluvial processes and therefore classified as Cambisols (Colluvic)(Figure 2 and S4). Locally, soil depth exceeded 50 cm, possibly reflecting small-scale variability in the topography of the parent material. No consistent trends in soil depth were observed, and there were no surface indicators that could be used to anticipate deeper soils. In both sites, local oozing zones with Histic Leptosols and specific plant community types were observed (Figure S1).

By comparing plain and slope areas, we found that variability in soil depth and the diversity of soil types were more pronounced on the plain than on the slope. We argue that the higher diversity of soil types on the plain arises from the variability of soil moisture content, as corresponding fen habitats (Delarze et al., 2015) often present a high diversity in hydrological processes and soil types (Gobat et al., 2013). Overall, our results highlight the interactive effect of topographic

position, parent material and pedoclimate on soil properties and ultimately on soil type diversity in subalpine environments (Figure 6). The spatial proximity of these soil types raises questions on the links between post-glacial landscape evolution and heterogeneity of the underlying parent material, especially variations in its distance to the soil surface, particle size distribution and resulting permeability.

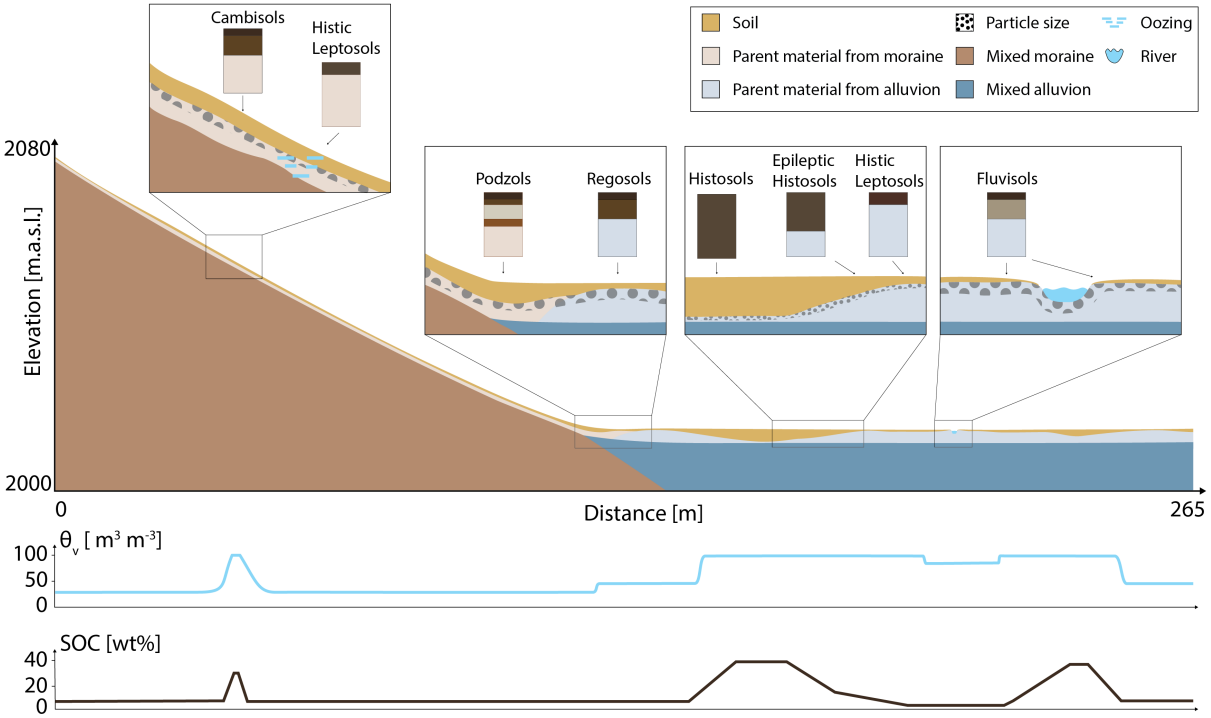

Figure 6: Conceptual slope–plain transect showing how the distribution of soils, parent materials and soil moisture content influences soil organic carbon (SOC) concentration. Reference soil groups with representative profiles are shown in relation to moraine- and alluvium-derived parent materials, including particle-size variations, topographic position and distance from the river. Lower panels illustrate spatial patterns of volumetric soil moisture content (θ_v, m^3 m^{-3}) and SOC concentration (wt%) along the transect. Higher soil moisture content on the plain leads to the formation of organic horizons and larger accumulation of SOC compared to the slope. On the plain, the variability in parent material controls soil depth, soil moisture patterns and consequently soil type distribution, ultimately driving SOC spatial distribution.

4.2 SOC concentrations are higher on plains than on slopes, with stronger within-plain contrasts linked to soil type

SOC concentrations in the top 50 cm were higher on the plain than on the slope. This pattern is consistent with the contrasting soil types associated with each topographic position and with

the habitat differences reflected by the plant community types. The highest SOC concentrations measured in the plain (58 wt%) were comparable with values measured in other fens and wetlands (Liebner et al., 2012; Nahlik and Fennessy, 2016), while the lower SOC concentrations measured on the slope were typical of alpine grasslands (Leifeld et al., 2009; Matteodo et al., 2018; Wasner et al., 2024) and heathland (Thaysen et al., 2017). Notably, we reported the lowest SOC concentration on the plain, on a sampling location assigned to Fluvisols (Fierz et al., 1995; Salomé et al., 2011; Santos et al., 1997). This underscores the wide within-plain range in SOC concentrations and its close association with soil type. SOC concentrations decreased with depth on the slope but not on the plain. This pattern reflects the relative homogeneity of soil type on the slope, whereas on the plain, the larger variation in soil type shaped SOC depth trends. For instance, Histosols and Epileptic Histosols both feature an organic-rich histic layer in the upper part of their profiles, but below 30 cm, the Epileptic Histosols have a mineral layer, whereas the Histosols remain organic-rich (Figure 6). Consistent with this contrast, elemental composition showed the strongest differentiation between topographic positions among measured soil properties. Higher Si, Al, Fe, K, Mn and P contents on the slope relative to the plain reflect the predominantly mineral nature of slope soils, whereas the plain is dominated by organic-rich soils. Only Ca, S and Cl were higher on the plain compared to the slope. Ca likely reflects local inputs from sedimentary rocks, while S and Cl may be linked to organic sources and water accumulation, respectively (Scherer, 2009; White, 2001). The proportion of clay-sized particles was higher on the slope, which is consistent with greater mineral weathering and potential in-situ clay formation compared to waterlogged, organic-rich soils, where conditions are less favourable for clay formation (Egli and Mirabella, 2021). Nevertheless, clay concentrations on plains ($\sim$ 3 % v v^{-1}) and on slopes ($\sim$ 4 % v v^{-1}) were on the lower end of the range reported for subalpine soils (Egli et al., 2001; Egli et al., 2008; Ferré et al., 2023). Across our study sites, SOC concentration, soil moisture and elemental composition differed significantly between topographic positions. While topography clearly shaped soil formation, producing contrasted soils and soil properties between plain and slope (organic vs. mineral), it did not fully capture the variability in SOC concentrations observed at the landscape scale.

4.3 Mineral content drives SOC variability, with secondary effects of sedimentary inputs and texture at fine spatial scales

To identify the mechanisms controlling landscape-scale variability in SOC concentrations, we fitted a model using predictors extracted factor analysis of the soil physicochemical dataset: mineral content, sedimentary rock influence, and a texture index. Mineral content captured the dominant gradient from organic-rich soils (negative mineral content values) to mineral-rich soils (positive mineral content values). The organic-rich end was characterised by higher S concentrations and higher C:N ratios, both positively associated with soil organic matter (Figure S7). The mineral-rich end showed higher Si, K and Al concentrations, consistent with the felsic parent materials at both sites (e.g. muscovite-rich gneiss in the Lirec formation in Ar du Tsan and Monte Leone strata in Blatt; Carrupt, 2003; Marthaler et al., 2008). In the field, mineral content values reflected topographic position and soil type. The slope, dominated by Cambisols, showed limited contrasts across locations and depths (mineral content between -1 and 1), whereas the plain spanned the full range of soil types and mineral content values (from Histosols at mineral content = -2.1 to Fluvisols mineral content = 1.15), with contrasts increasing with depth as profiles became more differentiated (e.g. Histosols vs. Epihistic Leptosols; Figure S8). Consistent with this structure, mineral content was the strongest driver of SOC concentrations, with higher SOC concentrations at lower mineral content. Although this effect is partly aligned with topographic position through soil type (organic-rich soils occurring mainly on the plain), topographic position alone had low predictive power because SOC variability was large within topographic positions, especially on the plain. Topographic positions fail to capture the fine-scale terrain variations that might drive SOC spatial distribution (Patton et al., 2019). Yet, high-resolution topography analysis is a proxy for SOC variability when the topography itself is varied. In topographically uniform areas, such as plains, SOC variability may be high due to shifts in soil type or moisture regimes, even when topographic variability is negligible.

Sedimentary rock influence was defined by high Ca and Mg concentrations and higher pH, and mapped onto Fluviosols and zones affected by sediment inputs from dolomite outcrops (Figure S9). The correlation between Ca/Mg and pH suggests that the dissolution of sedimentary rocks releases carbonates and leads to an increase in pH. Sedimentary rock influence was the

second-best predictor for SOC variability at the landscape scale, with SOC concentrations decreasing as sedimentary rock influence increased. This pattern was largely driven by Fluvisols, which combined high sedimentary rock influence with low SOC concentrations. Importantly, sedimentary rock influence differed from mineral content by reflecting the origin of mineral inputs (sedimentary vs. igneous) and was essentially uncorrelated with mineral content in the factor analysis, pointing to an additional control linked to transport: easily eroded sedimentary material is redistributed and contributes to Fluvisol formation where transport is strongest on the plain.

Texture index summarises particle-size distribution in a fine-to-coarse texture gradient. We did not observe a clear spatial pattern in the texture index beyond a higher frequency of fine-textured samples on the slope (Figure S10), consistent with higher clay proportions (Figure 3B). Texture index was the weakest continuous predictor of SOC concentration (Figure 4), displaying a negative correlation where increasing texture index values—indicative of finer soil textures—corresponded with declining SOC concentration. While this deviates from the consensus on the stabilising role of clay-sized particles for SOC, it is consistent with observations of Ferré et al. (2020), who found that coarser texture coincided with low topographic position and elevated SOC concentrations. In the present study, this trend is driven by a distinct landscape contrast: well-drained slopes characterised by higher clay proportions and lower SOC concentrations, versus partially waterlogged plains featuring coarser textures and higher SOC accumulation. However, we do not expect soil texture to have a significant effect on SOC content, as the proportion of clay in our study sites is low and the difference in clay proportion across topographic positions are small (1.78% v v^{-1} higher on slopes than on plains). Our results show that SOC accumulation was driven primarily by high soil moisture driving the formation of organic layers, rather than the association of SOC with minerals.

Among the fixed effects, soil type showed low predictive capacity for SOC concentration. While soil type can improve SOC predictions in other contexts, its effect here was likely subsumed by mineral content, because most soil-type differences across our sites are fundamentally linked to the presence/absence and thickness of histic layers and thus to the mineral–organic continuum captured by mineral content. Mineral content might have also shadowed the effect of soil type on

SOC concentration in the linear mixed-effect model, as continuous predictors inherently describe continuous response variables better than categorical predictors, especially when a strong linear trend is evident (Figure 5). Nevertheless, soil types reflect distinct pedogenic trajectories and SOC accumulation histories (Kögel-Knabner and Amelung, 2021), and the much higher soil-type diversity on the plain aligns with its stronger SOC variability. Together, these results highlight a limitation of a simple toposequence (catena) approach: a single "plain" position can include multiple hydrological and pedogenic settings. This supports the need for high sampling resolution—even over relatively small areas—in alpine and other highly heterogeneous landscapes, where extrapolating SOC stocks from sparse sampling can produce biased estimates of SOC concentration.

5 Conclusion

We found that SOC concentration is inversely related to soil mineral content, as this factor best captured the gradient of organic-rich to mineral-rich soils present across plain and slope positions. This suggests that SOC accumulation is primarily driven by hydrologically-induced oxygen limitations rather than stabilization through organo-mineral associations. While topography modulates the environmental conditions for SOC accumulation, it remains an incomplete predictor of SOC concentration due to high soil type diversity within topographic positions. The coexistence of organic Histosols and mineral-rich Fluvisols on the plains highlights that soil moisture-driven soil type diversity provides a more precise framework for understanding organic carbon distribution than topographic position alone. Relying strictly on topographic classifications may overlook important nuances in soil property distribution. We propose that soil type is a more robust predictor of SOC variability at the landscape scale, as it integrates the mineralogical gradients and depth-dependent processes that drive SOC dynamics. Ultimately, accurately quantifying SOC stocks in heterogeneous subalpine environments requires high-resolution sampling. Such an approach may better account for the high soil heterogeneity found in subalpine environments, where post-glacial landscape evolution partly controls the interplay of topography, parent material and pedoclimate and their effect on SOC accumulation.

Acknowledgements

We thank the Swiss National Science Foundation for financial support (Grant No. 212056), Pascal Vittoz for recommending the study sites, and the municipalities of Binn and Chalais, and the canton of Wallis for allowing access to the study sites. We also thank Laetitia Monbaron and Brahimsamba Bomou for technical support in the laboratories of the University of Lausanne, and Eric Pizem, Antoine Wallart and Romain Castro for their help with field and laboratory work.

References

Arrouays, D., Deslais, W., & Badeau, V. (2001). The carbon content of topsoil and its geographical distribution in France. *Soil Use and Management*, *17*(1), 7–11. https://doi.org/10.1111/j.1475-2743.2001.tb00002.x

Bai, Y., & Zhou, Y. (2020). The main factors controlling spatial variability of soil organic carbon in a small karst watershed, Guizhou Province, China. *Geoderma*, *357*, 113938. https://doi.org/10.1016/j.geoderma.2019.113938

Baize, D., & Girard, M.-C. (2008). *Référentiel pédologique 2008*. QUAE.

Bell, M. J., & Worrall, F. (2009). Estimating a region's soil organic carbon baseline: The undervalued role of land-management. *Geoderma*, *152*(1), 74–84. https://doi.org/10.1016/j.geoderma.2009.05.020

Birkeland, P. W. (1999). *Soils and geomorphology* (3rd). Oxford University Press, Inc.

Carrupt, E. (2003). *New stratigraphic, structural and geochemical data from the Val Formazza - Binntal area (Central Alps)* [Mémoire de Géologie (Lausanne)]. Université de Lausanne.

Delarze, R., Gonseth, Y., Eggenberg, S., & Vust, M. (2015). *Guide mes milieux naturels de Suisse* (3ème). Rissolis.

Dickopp, J., Lengerer, A., & Kazda, M. (2018). Relationship between groundwater levels and oxygen availability in fen peat soils. *Ecological Engineering*, *120*, 85–93. https://doi.org/10.1016/j.ecoleng.2018.05.033

Egli, M., Mirabella, A., & Fitze, P. (2001). Clay mineral formation in soils of two different chronosequences in the Swiss Alps. *Geoderma*, *104*(1), 145–175. https://doi.org/10.1016/S0016-7061(01)00079-9

Egli, M., Merkli, C., Sartori, G., Mirabella, A., & Plötze, M. (2008). Weathering, mineralogical evolution and soil organic matter along a Holocene soil toposequence developed on carbonate-rich materials. *Geomorphology*, *97*(3), 675–696. https://doi.org/10.1016/j.geomorph.2007.09.011

Egli, M., & Mirabella, A. (2021, January 21). The Origin and Formation of Clay Minerals in Alpine Soils. In A. Hunt, M. Egli, & B. Faybishenko (Eds.), *Geophysical Monograph Series* (1st ed., pp. 121–137). Wiley. https://doi.org/10.1002/9781119563952.ch6

Ferré, C., Caccianiga, M., Zanzottera, M., & Comolli, R. (2020). Soil–plant interactions in a pasture of the Italian Alps. *Journal of Plant Interactions*, *15*(1), 39–49. https://doi.org/10.1080/17429145.2020.1738570

Ferré, C., Mascetti, G., Gentili, R., Citterio, S., & Comolli, R. (2023). Soil climate regulation services: High SOC stock in Podzols and Umbrisols in an alpine grassland (Valle Adamé, Italy). *Environmental Earth Sciences*, *82*(22), 534. https://doi.org/10.1007/s12665-023-11228-z

Fierz, M., Gobat, J., & Guenat, C. (1995). Quantification et caractérisation de la matière organique de sols alluviaux au cours de l'évolution de la végétation. *Annales des Sciences Forestières*, *52*(6), 547–559. https://doi.org/10.1051/forest:19950603

Françoys, A., Li, H., Mendoza, O., Dewitte, K., Bodé, S., Boeckx, P., Cornelis, W., De Neve, S., & Sleutel, S. (2024). Control of landscape position on organic matter decomposition via soil moisture during a wet summer. *Soil and Tillage Research*, *244*, 106277. https://doi.org/10.1016/j.still.2024.106277

Freléchoux, F., & Gallandat, J.-D. (1995). Flore et végétation du haut Val de Binn entre Chiestafel et le col de l'Albrun. *Bulletin de la Murithienne*, (113), 105–128.

Garcia-Pausas, J., Casals, P., Camarero, L., Huguet, C., Sebastià, M.-T., Thompson, R., & Romanyà, J. (2007). Soil organic carbon storage in mountain grasslands of the Pyrenees: Effects of climate and topography. *Biogeochemistry*, *82*(3), 279–289. https://doi.org/10.1007/s10533-007-9071-9

Gobat, J.-M., Aragno, M., & Matthey, W. (2013). *Le sol vivant - Bases de pédologie, biologie des sols* (troisème édition). Presses polytechniques et universitaires romandes.

Hoffmann, U., Hoffmann, T., Jurasinski, G., Glatzel, S., & Kuhn, N. (2014). Assessing the spatial variability of soil organic carbon stocks in an alpine setting (Grindelwald, Swiss Alps). *Geoderma*, *232–234*, 270–283. https://doi.org/10.1016/j.geoderma.2014.04.038

Kleber, M., Eusterhues, K., Keiluweit, M., Mikutta, C., Mikutta, R., & Nico, P. S. (2015, January 1). Chapter One - Mineral–Organic Associations: Formation, Properties, and Relevance in Soil Environments. In D. L. Sparks (Ed.), *Advances in Agronomy* (pp. 1–140, Vol. 130). Academic Press. https://doi.org/10.1016/bs.agron.2014.10.005

Kögel-Knabner, I., & Amelung, W. (2021). Soil organic matter in major pedogenic soil groups. *Geoderma*, *384*, 114785. https://doi.org/10.1016/j.geoderma.2020.114785

Kopecký, M., Macek, M., & Wild, J. (2021). Topographic Wetness Index calculation guidelines based on measured soil moisture and plant species composition. *Science of The Total Environment*, *757*, 143785. https://doi.org/10.1016/j.scitotenv.2020.143785

Körner, C. (2021). Alpine soils. In C. Körner (Ed.), *Alpine Plant Life: Functional Plant Ecology of High Mountain Ecosystems* (pp. 119–140). Springer International Publishing. https://doi.org/10.1007/978-3-030-59538-8_6

Leifeld, J., Zimmermann, M., Fuhrer, J., & Conen, F. (2009). Storage and turnover of carbon in grassland soils along an elevation gradient in the Swiss Alps. *Global Change Biology*, *15*(3), 668–679. https://doi.org/10.1111/j.1365-2486.2008.01782.x

Liebner, S., Schwarzenbach, S. P., & Zeyer, J. (2012). Methane emissions from an alpine fen in central Switzerland. *Biogeochemistry*, *109*(1), 287–299. https://doi.org/10.1007/s10533-011-9629-4

Luo, B., Li, J., Tang, J., Wei, C., & Zhong, S. (2024). Microtopography effects on pedogenesis in the mudstone-derived soils of the hilly mountainous regions. *Scientific Reports*, *14*(1), 11998. https://doi.org/10.1038/s41598-024-62540-y

Mair, P., & Wilcox, R. (2014). WRS2: A Collection of Robust Statistical Methods, 1.1–7. https://doi.org/10.32614/CRAN.package.WRS2

Man, M., Kalčík, V., Macek, M., Brůna, J., Hederová, L., Wild, J., & Kopecký, M. (2023). myClim: Microclimate data handling and standardised analyses in R. *Methods in Ecology and Evolution*, *14*(9), 2308–2320. https://doi.org/10.1111/2041-210X.14192

Marthaler, M., Sartori, M., & Escher, A. (2008). *Vissoie* (122 = 122). Bundesamt für Landestopografie swisstopo.

Matteodo, M., Grand, S., Sebag, D., Rowley, M. C., Vittoz, P., & Verrecchia, E. P. (2018). Decoupling of topsoil and subsoil controls on organic matter dynamics in the Swiss Alps. *Geoderma*, *330*, 41–51. https://doi.org/10.1016/j.geoderma.2018.05.011

Nahlik, A. M., & Fennessy, M. S. (2016). Carbon storage in US wetlands. *Nature Communications*, *7*(1), 13835. https://doi.org/10.1038/ncomms13835

Nakagawa, S., & Schielzeth, H. (2013). A general and simple method for obtaining R2 from generalized linear mixed-effects models. *Methods in Ecology and Evolution*, *4*(2), 133–142. https://doi.org/10.1111/j.2041-210x.2012.00261.x

Patton, N. R., Lohse, K. A., Seyfried, M. S., Godsey, S. E., & Parsons, S. B. (2019). Topographic controls of soil organic carbon on soil-mantled landscapes. *Scientific Reports*, *9*(1), 6390. https://doi.org/10.1038/s41598-019-42556-5

Pinheiro, J., Bates, D., & R Core Team. (2025). *Nlme: Linear and nonlinear mixed effects models* [R package version 3.1-168]. https://CRAN.R-project.org/package=nlme

Poulenard, J., & Podwojewski, P. (2005). Alpine Soils. In *Encyclopedia of Soil Science - Two-Volume Set* (2nd ed.). CRC Press.

Richard, J.-L., Bressoud, B., Buttler, A., Duckert, O., & Gallandat, J.-D. (1993). Carte de la végétation de la région val de Réchy-Sassenèire. *Bulletin de la Murithienne*, (111), 9–40.

Salomé, C., Guenat, C., Bullinger-Weber, G., Gobat, J.-M., & Le Bayon, R.-C. (2011). Earthworm communities in alluvial forests: Influence of altitude, vegetation stages and soil parameters. *Pedobiologia*, *54*, S89–S98. https://doi.org/10.1016/j.pedobi.2011.09.012

Santos, M. L. M., Guenat, C., Thevoz, C., Bureau, F., & Vedy, J. C. (1997). Impacts of Embanking on the Soil-Vegetation Relationships in a Floodplain Ecosystem of a Pre-Alpine River. *Global Ecology and Biogeography Letters*, *6*(3/4), 339–348. https://doi.org/10.2307/2997748

Scherer, H. W. (2009). Sulfur in soils. *Journal of Plant Nutrition and Soil Science*, *172*(3), 326–335. https://doi.org/10.1002/jpln.200900037

Thaysen, E. M., Reinsch, S., Larsen, K. S., & Ambus, P. (2017). Decrease in heathland soil labile organic carbon under future atmospheric and climatic conditions. *Biogeochemistry*, *133*(1), 17–36. https://doi.org/10.1007/s10533-017-0303-3

Wasner, D., Abramoff, R., Griepentrog, M., Venegas, E. Z., Boeckx, P., & Doetterl, S. (2024). The Role of Climate, Mineralogy and Stable Aggregates for Soil Organic Carbon Dynamics Along a Geoclimatic Gradient. *Global Biogeochemical Cycles*, *38*(7), e2023GB007934. https://doi.org/10.1029/2023GB007934

White, P. J. (2001). Chloride in Soils and its Uptake and Movement within the Plant: A Review. *Annals of Botany*, *88*(6), 967–988. https://doi.org/10.1006/anbo.2001.1540

Wiesmeier, M., Barthold, F., Spörlein, P., Geuß, U., Hangen, E., Reischl, A., Schilling, B., Angst, G., von Lützow, M., & Kögel-Knabner, I. (2014). Estimation of total organic carbon storage and its driving factors in soils of Bavaria (southeast Germany). *Geoderma Regional*, *1*, 67–78. https://doi.org/10.1016/j.geodrs.2014.09.001

Wilcox, R. R. (2022). *Introduction to robust estimation and hypothesis testing* (Fifth edition). Academic Press, an imprint of Elsevier.

Wild, J., Kopecký, M., Macek, M., Šanda, M., Jankovec, J., & Haase, T. (2019). Climate at ecologically relevant scales: A new temperature and soil moisture logger for long-term microclimate measurement. *Agricultural and Forest Meteorology*, *268*, 40–47. https://doi.org/10.1016/j.agrformet.2018.12.018

William Revelle. (2025). *Psych: Procedures for psychological, psychometric, and personality research* [R package version 2.5.6]. Northwestern University. Evanston, Illinois. https://CRAN.R-project.org/package=psych

WRB, I. W. G. (2022). *World Reference Base for Soil Resources. International soil classification system for naming soils and creating legends for soil maps.* (4th ed.). International Union of Soil Sciences (IUSS), Vienna, Austria.

Zhu, M., Feng, Q., Zhang, M., Liu, W., Qin, Y., Deo, R. C., & Zhang, C. (2019). Effects of topography on soil organic carbon stocks in grasslands of a semiarid alpine region, northwestern China. *Journal of Soils and Sediments*, *19*(4), 1640–1650. https://doi.org/10.1007/s11368-018-2203-0

Supplementary Information for:

Interactive effects of landscape position and soil diversity drive the spatial variability of soil organic carbon concentration in subalpine soils of Switzerland

Dienes, B.[1], Mendoza, O.[1,2], Bright, K.[1], Licini, G.[1], Aeppli, M.[1,*]

[1]Soil Biogeochemistry laboratory (SOIL), Swiss Federal Institute of Technology Lausanne (EPFL), Sion, Switzerland

[2]Institute of Earth Surface Dynamics, Faculty of Geosciences and the Environment, University of Lausanne, Lausanne, Switzerland

[*] correspondence: meret.aeppli@epfl.ch, +41 21 693 72 79

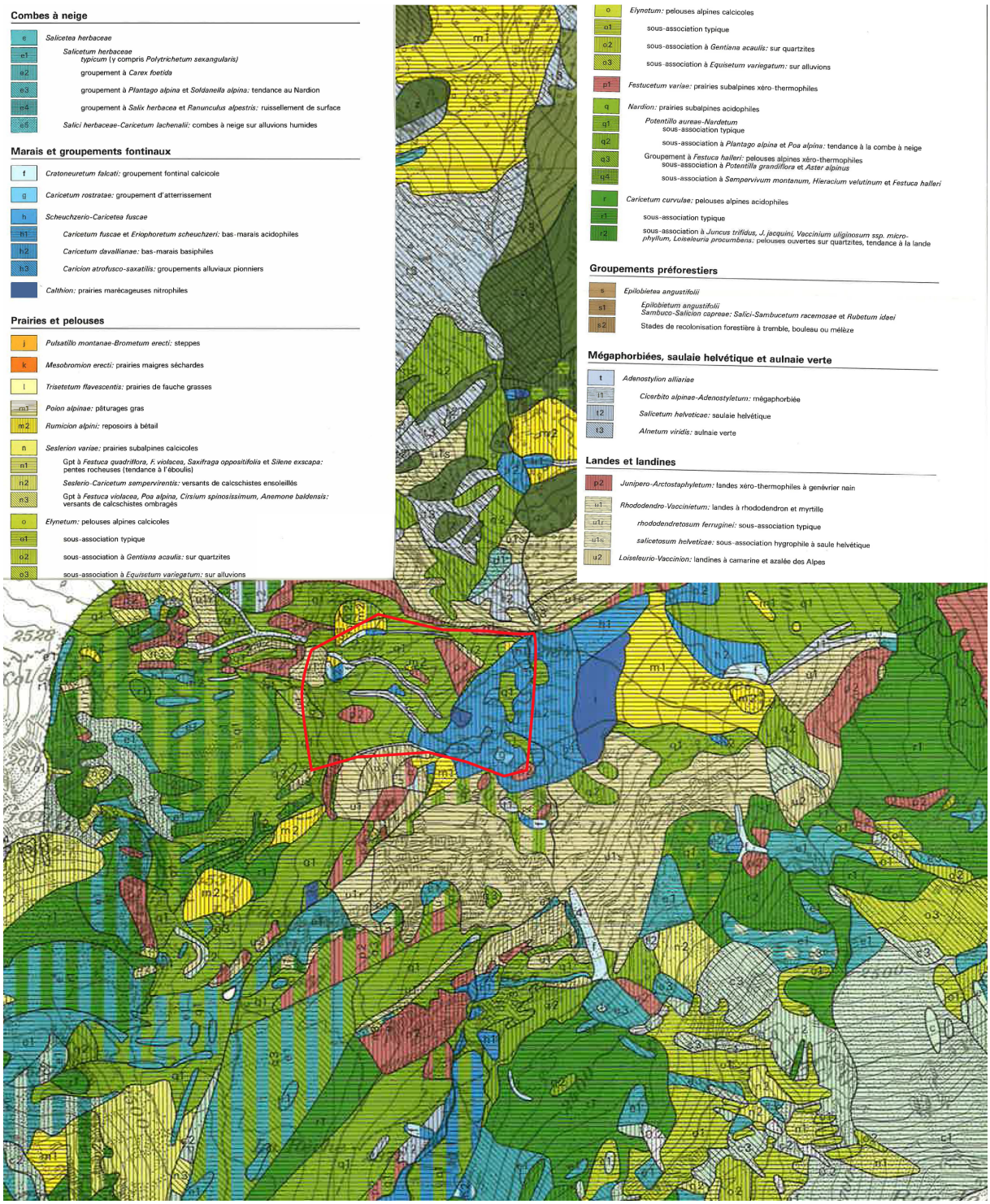

Figure S1: Map of plant community types in Ar du Tsan and lower Vallon de Réchy. The map is from Richard et al. (1993). The study area is highlighted by the red polygon.

Vegetation map - Blatt

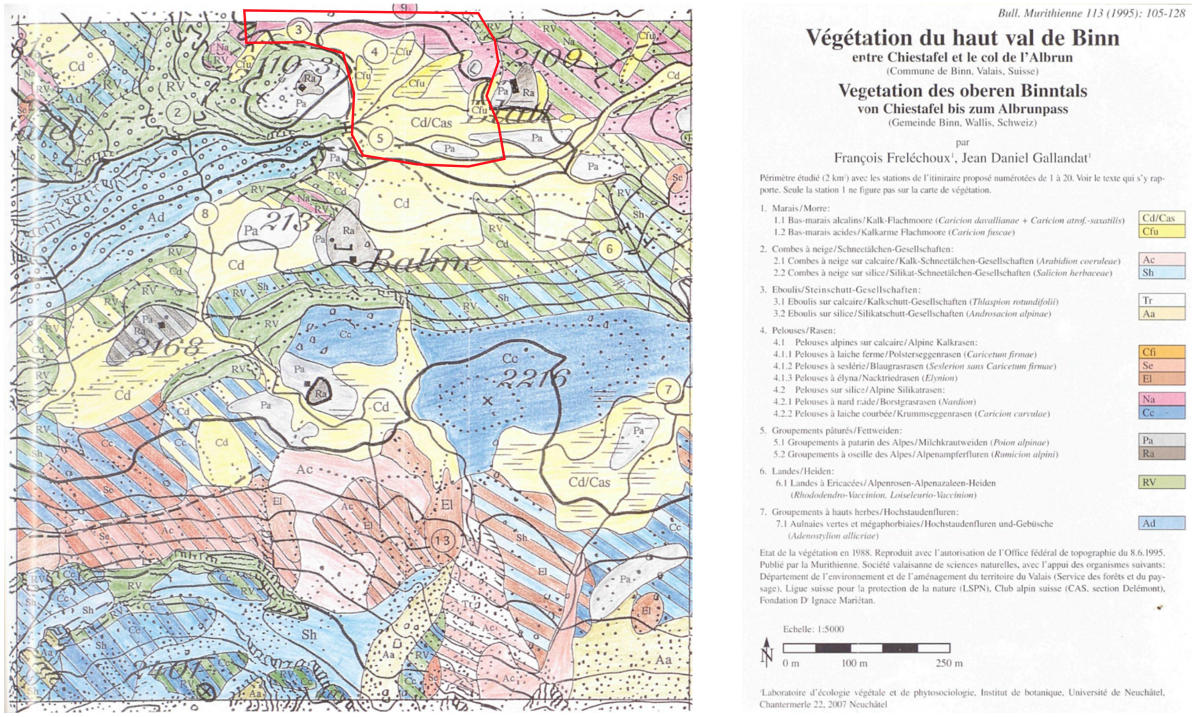

Figure S2: Map of plant community types in Blatt and lower Binntal. The map is from Freléchoux and Gallandat (1995). The study area is highlighted by the red polygon. Only the lower part of the slope appears on the vegetation map.

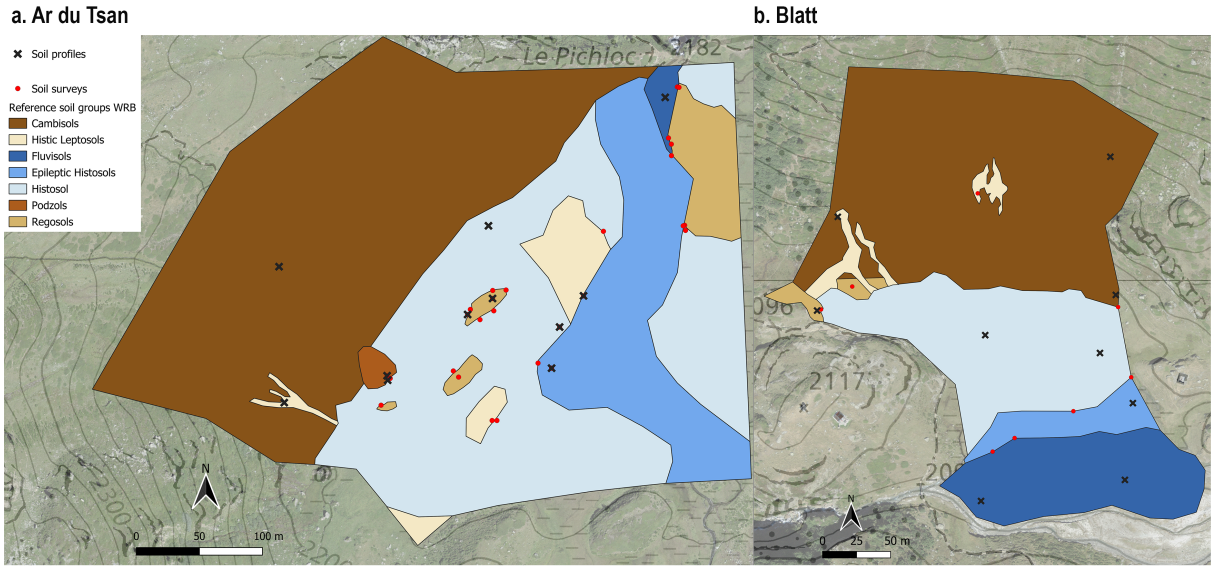

Figure S3: Map of soil profiles (black cross) and soil surveys (red dot) overlapping the map of Reference soil groups (WRB). Panels show the map for Ar du Tsan (a) and Blatt (b) overlaid on an orthophoto and a topographic (1:10'000) basemap from Swisstopo.

Table S1: Summary table of soil moisture and temperature data

Name	Catchment	Topographic position	Latitude [°N]	Longitude [°E]	Temperature at 10 cm [°C]	Temperature at 30 cm [°C]	Soil moisture at 10 cm [°C]	Soil moisture at 30 cm [°C]
RT1.1	Ar du Tsan	Plain	46.199973	7.508809	5.02	NA	1.00	1.00
RT1.2	Ar du Tsan	Plain	46.200135	7.508162	5.15	4.89	0.27	0.28
RT1.3	Ar du Tsan	Plain	46.200244	7.507488	4.87	4.73	0.32	0.38
RT1.4	Ar du Tsan	Slope	46.200487	7.506815	5.98	6.03	0.38	0.29
RT1.5	Ar du Tsan	Slope	46.200676	7.506297	6.03	5.96	0.41	0.40
RT1.6	Ar du Tsan	Slope	46.200901	7.505805	5.83	5.90	0.40	0.33
RT2.1	Ar du Tsan	Plain	46.200476	7.509108	4.96	4.78	1.00	1.00
RT2.2	Ar du Tsan	Plain	46.200594	7.508434	4.85	4.80	0.47	0.44
RT2.3	Ar du Tsan	Plain	46.200675	7.507851	5.44	5.42	1.00	1.00
RT2.4	Ar du Tsan	Slope	46.200990	7.507269	6.07	NA	0.49	NA
RT2.5	Ar du Tsan	Slope	46.201260	7.506868	6.09	5.96	0.35	0.33
RT2.6	Ar du Tsan	Slope	46.201486	7.506168	6.21	6.05	0.32	0.35
BT1.1	Blatt	Plain	46.380182	8.277323	4.94	4.95	0.95	1.00
BT1.2	Blatt	Plain	46.380713	8.277357	5.41	NA	1.00	1.00
BT1.3	Blatt	Plain	46.381064	8.277258	5.49	NA	0.90	1.00
BT1.4	Blatt	Slope	46.381541	8.277304	5.37	5.24	0.46	0.45
BT1.5	Blatt	Slope	46.382044	8.277364	5.88	5.49	0.39	0.34
BT1.6	Blatt	Slope	46.382566	8.277333	4.90	4.70	0.41	0.35
BT1.2.1	Blatt	Plain	46.380704	8.277292	5.23	NA	1.00	1.00
BT1.2.2	Blatt	Plain	46.380714	8.277097	4.86	5.04	0.77	0.99
BT1.4.1	Blatt	Slope	46.381540	8.277408	5.34	NA	0.49	0.43
BT1.4.2	Blatt	Slope	46.381548	8.277526	5.47	5.61	0.42	0.40
BT1.6.1	Blatt	Slope	46.382593	8.277321	5.38	4.61	0.38	0.31
BT1.6.2	Blatt	Slope	46.382573	8.277528	5.34	5.09	0.43	0.38

Figure S4: Soil profiles representative of the reference soil groups encountered across the study sites. Classifications following the Référentiel pédologique (RP) and tge World Reference Base (WRB) are provieded. GPS coordinates refer to the Swiss CH1903 coordinate system.

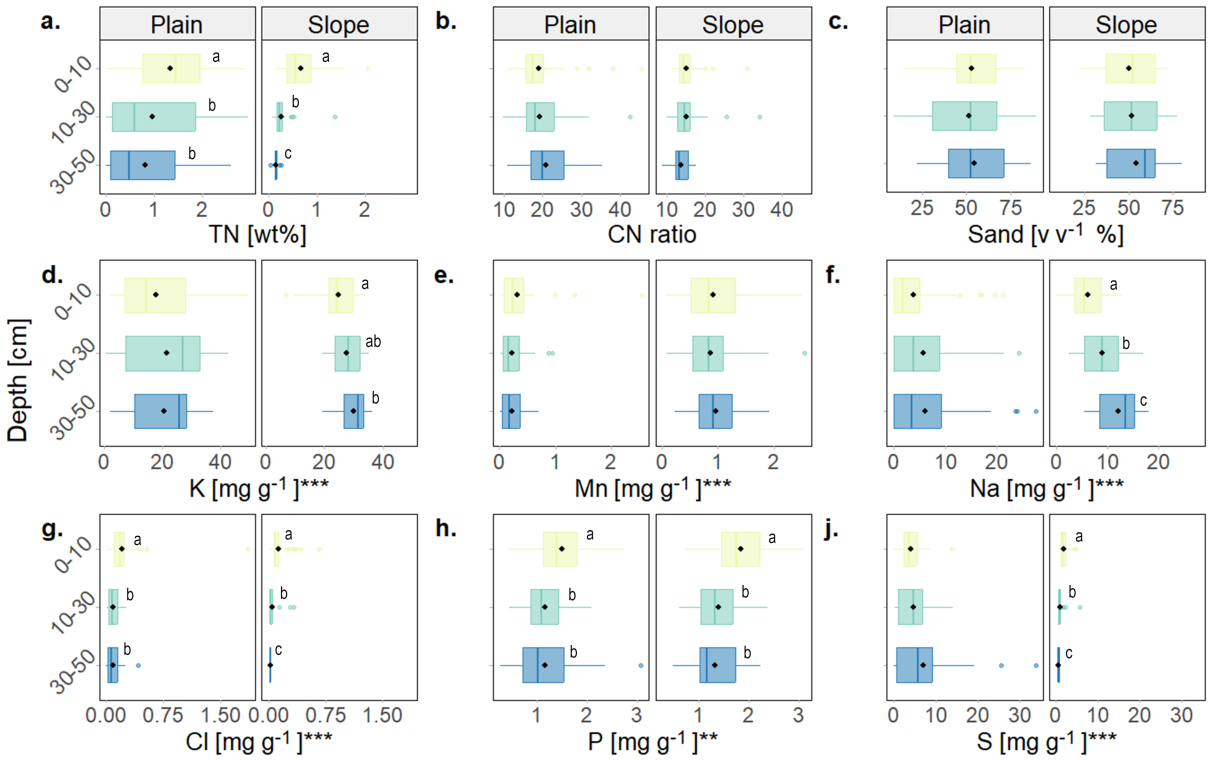

Figure S5: Depth profiles of soil physicochemical properties in plain and slope positions. Contents of **a.** Total nitrogen (TN). **b.** Carbon-to-Nitrogen ratio (CN). **c.** Sand. **d.** Potassium (K). **e.** Manganese (Mn). **f.** Sodium (Na). **g.** Chloride (Cl). **h.** Phosphorus (P). **i.** Sulphur (S). Black diamonds represent the box's mean. Significant differences between topographic positions are indicated by asterisks as follows <0.05(*), <0.01(**) and <0.001(***). Lowercase letters indicate significant differences among depths within the same topographic position. Values are given in mg g^{-1} of dry soil.

Table S2: Summary of factor analysis outputs

Loadings of all variables

Variables	Mineral content	Texture index	Sedimentary rock influence
Si	0.93	-0.09	-0.04
K	0.86	-0.09	0.13
Al	0.85	0.24	0.08
Na	0.74	-0.46	0.08
S	-0.7	0.1	0.1
Fe	0.67	0.38	0.07
Mn	0.55	0.17	-0.16
CN	-0.52	-0.22	0.12
Cl	-0.44	-0.07	-0.12
Sand	0.02	-1	-0.06
Silt	-0.03	0.96	0.08
Clay	0.11	0.76	-0.23
Mg	0.2	0.17	0.87
Ca	-0.2	-0.25	0.76
pH	0.05	0.01	0.72
P	0.21	-0.17	-0.43

Variance explained by factors

	Mineral content	Texture index	Sedimentary rock influence
Proportion variance	0.3	0.2	0.14
Cumulative variance	0.3	0.49	0.63

Correlation between factors

	Mineral content	Texture index	Sedimentary rock influence
Mineral content	1	0.11	0.19
Texture index	0.11	1	0.03
Sedimentary rock influence	0.19	0.03	1

Table S3: Summary table of linear mixed-effect model outputs

Fixed effects: C ∼ Soil type + Catchment + Topographic position + Depth + MC + TI + SRI + Catchment * Topo + Topo * Depth					
summary()					
	Value	Std.Error	DF	t-value	p-value
(Intercept)	14.22	1.13	144	12.563	0
SoilTypeWRB_corFluvisol	1.33	1.77	92	0.754	0.453
SoilTypeWRB_corHistic Leptosol	0.87	1.42	92	0.614	0.5409
SoilTypeWRB_corHistosols	2.88	1.25	92	2.313	0.023
SoilTypeWRB_corLeptic Cambisols (Colluvic)	3.72	2.13	92	1.743	0.0847
SoilTypeWRB_corRegosol	4.80	1.94	92	2.476	0.0151
CatchmentR	0.72	1.04	92	0.696	0.4883
TopoS	-4.71	2.20	92	-2.141	0.0349
DepthB	-1.67	0.73	144	-2.283	0.0239
DepthC	-2.56	0.82	144	-3.104	0.0023
SMC	-12.73	0.50	144	-25.260	0
Texture	-0.66	0.25	144	-2.678	0.0083
SRI	-2.17	0.44	144	-4.894	0
CatchmentR:TopoS	0.44	1.35	92	0.325	0.7461
TopoS:DepthB	0.87	1.02	144	0.861	0.3909
TopoS:DepthC	2.68	1.36	144	1.970	0.0508
anova.lme(type= ”marginal”)					
	numDF	denDF	F-value	p-value	
(Intercept)	1	144	157.825	¡.0001	
SoilTypeWRB_cor	5	92	2.756	0.0229	
Catchment	1	92	0.484	0.4883	
Topo	1	92	4.584	0.0349	
Depth	2	144	4.967	0.0082	
SMC	1	144	638.066	¡.0001	
Texture	1	144	7.172	0.0083	
SRI	1	144	23.954	¡.0001	
Catchment:Topo	1	92	0.106	0.7461	
Topo:Depth	2	144	1.942	0.1471	
Variances and R-squares					
	Random variance	Residual variance	R2 marginal	R2 conditional	
model	1.387842	12.98552	0.9329415	0.9394164	

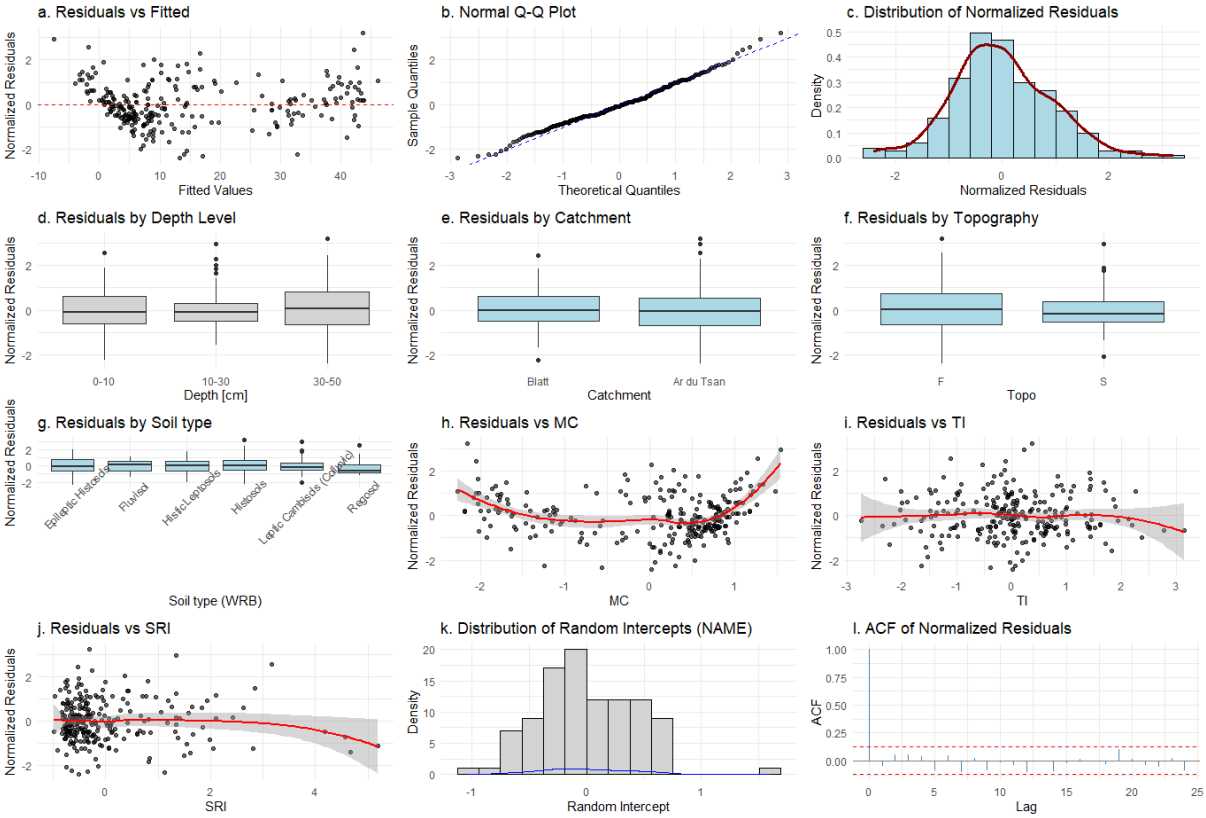

Figure S6: Diagnostic plots of the linear mixed-effect model. **a.** Residual vs Fitted, **b.** Normal Q-Q Plot, **c-g.** heteroscedasticity by categorical variables, **h-j.** Residuals vs continuous predictors, **k.** Distribution of Random intercepts, **l.** ACF of normalised residuals.

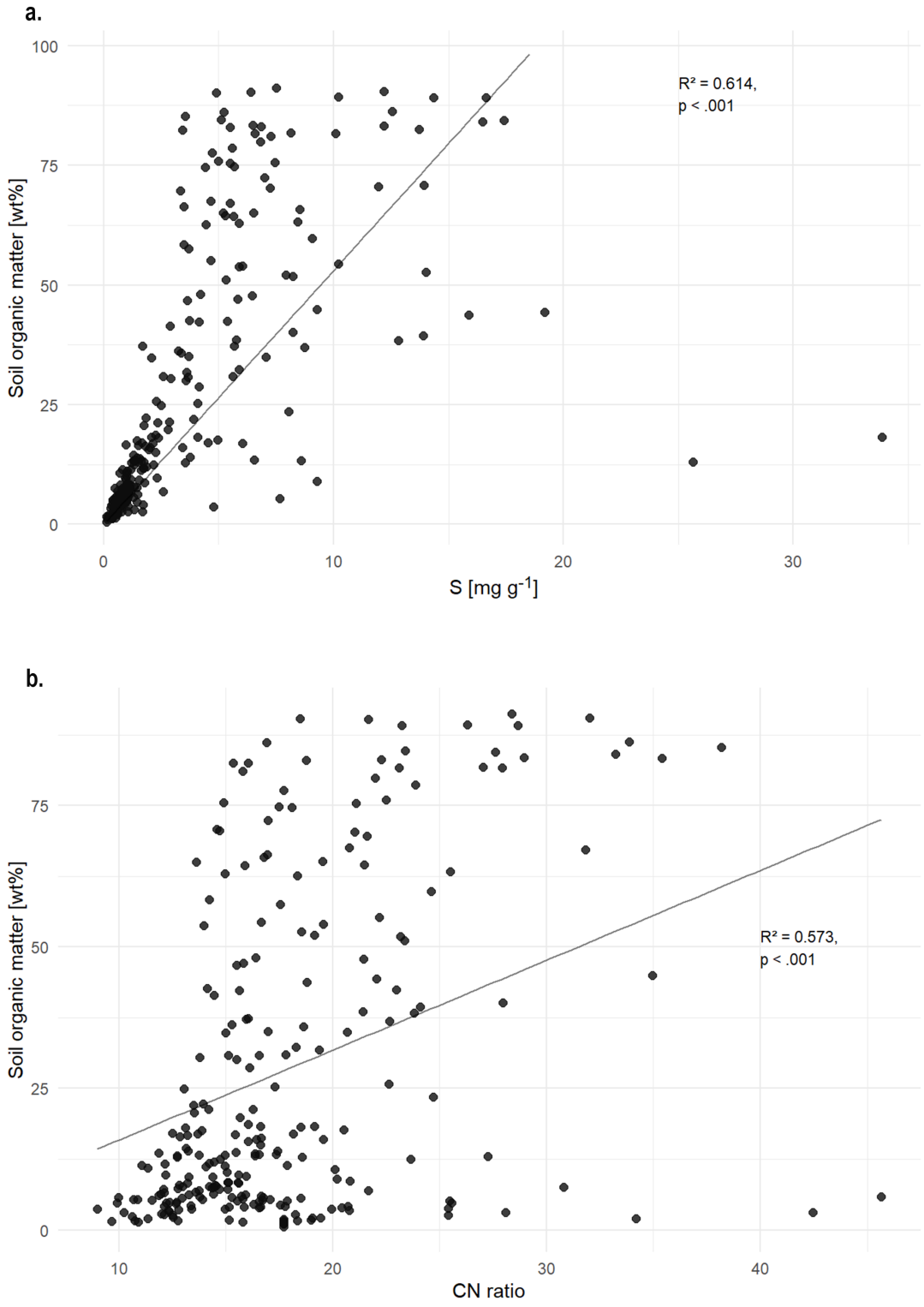

Figure S7: Relationship between **a.** soil organic matter (SOM) and sulphur, **b.** SOM and the carbon-to-nitrogen ratio (CN ratio). The solid line represents the fitted linear regression between SOM and S ($R^2 = 0.61$, $p < .001$) and between SOM and CN ratio($R^2 = 0.57$, $p < .001$).

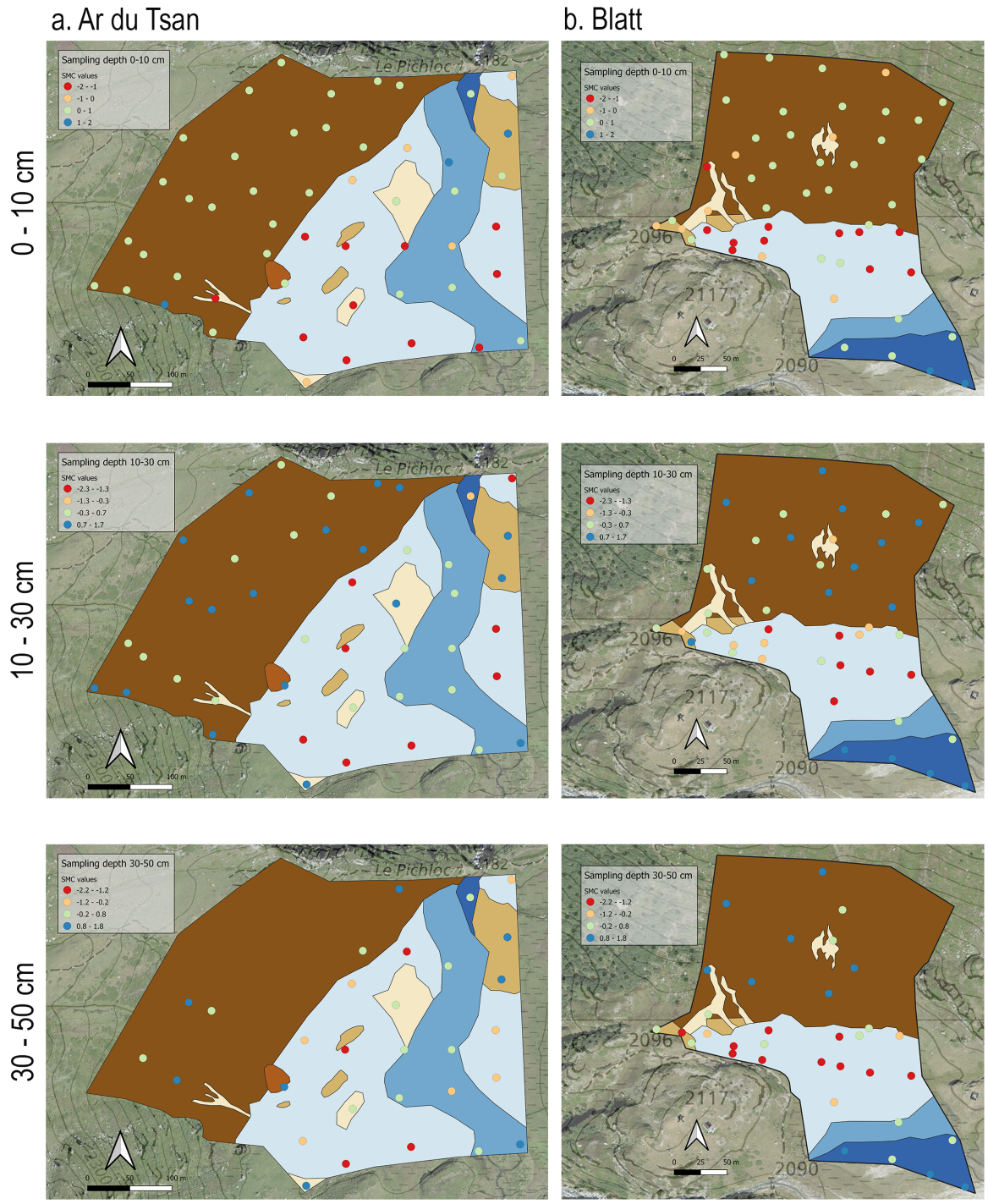

Figure S8: Map of mineral content values derived from the factor analysis overlapping the map of Reference soil groups (WRB). Left panels show the evolution of these values with depth for Ar du Tsan, when right panels show the evolution for Blatt. The base map is an orthophoto overlaid on a topographic map (1:10'000) from Swisstopo.

a. Ar du Tsan

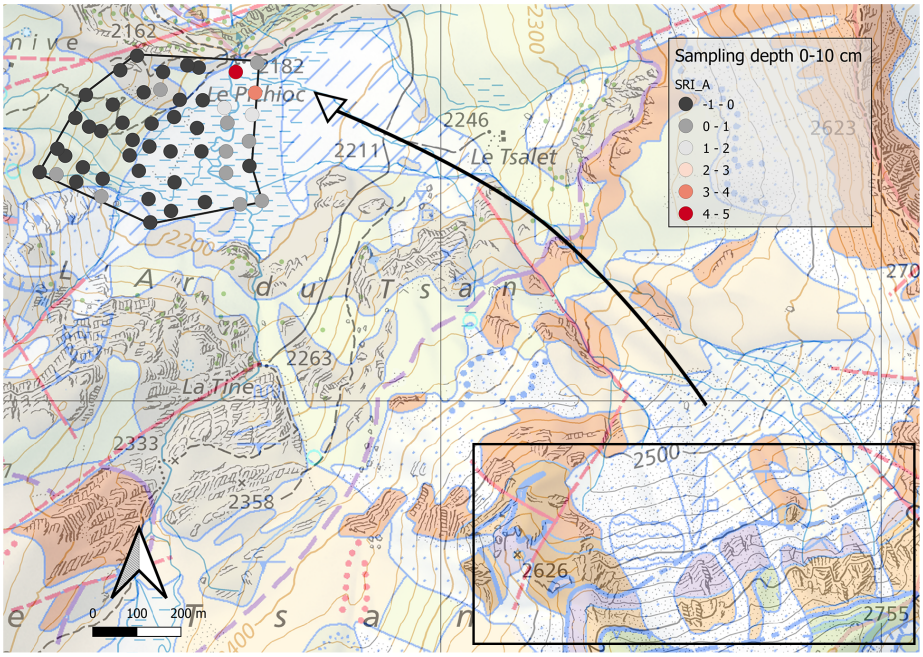

b. Blatt

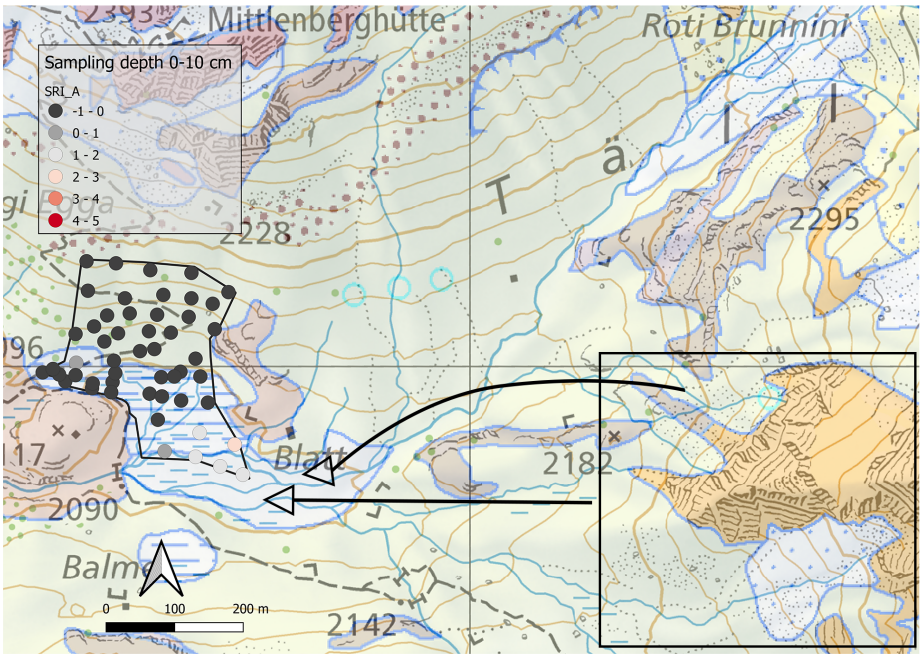

Figure S9: Map of the origin of sedimentary rock inputs and its effect on the values of sedimentary rock influence at depth of 0-10 cm, with higher values indicating higher sedimentary rock influence. Black squares highlight the main zone of sedimentary rock outcrops, and black arrows show the direction of transport by streams to the study sites. In **a.** Ar du Tsan, the orange formations are cornieule, conglomerate conatining limestone and dolomite, the purple one is argillite containing limestone, and the green one is marble. In **b.** Blatt, the orange formation is dolomite and the purple one is limestone-shale. The base map is a topographic map (1:10'000) overlaid by the geology map from Swisstopo

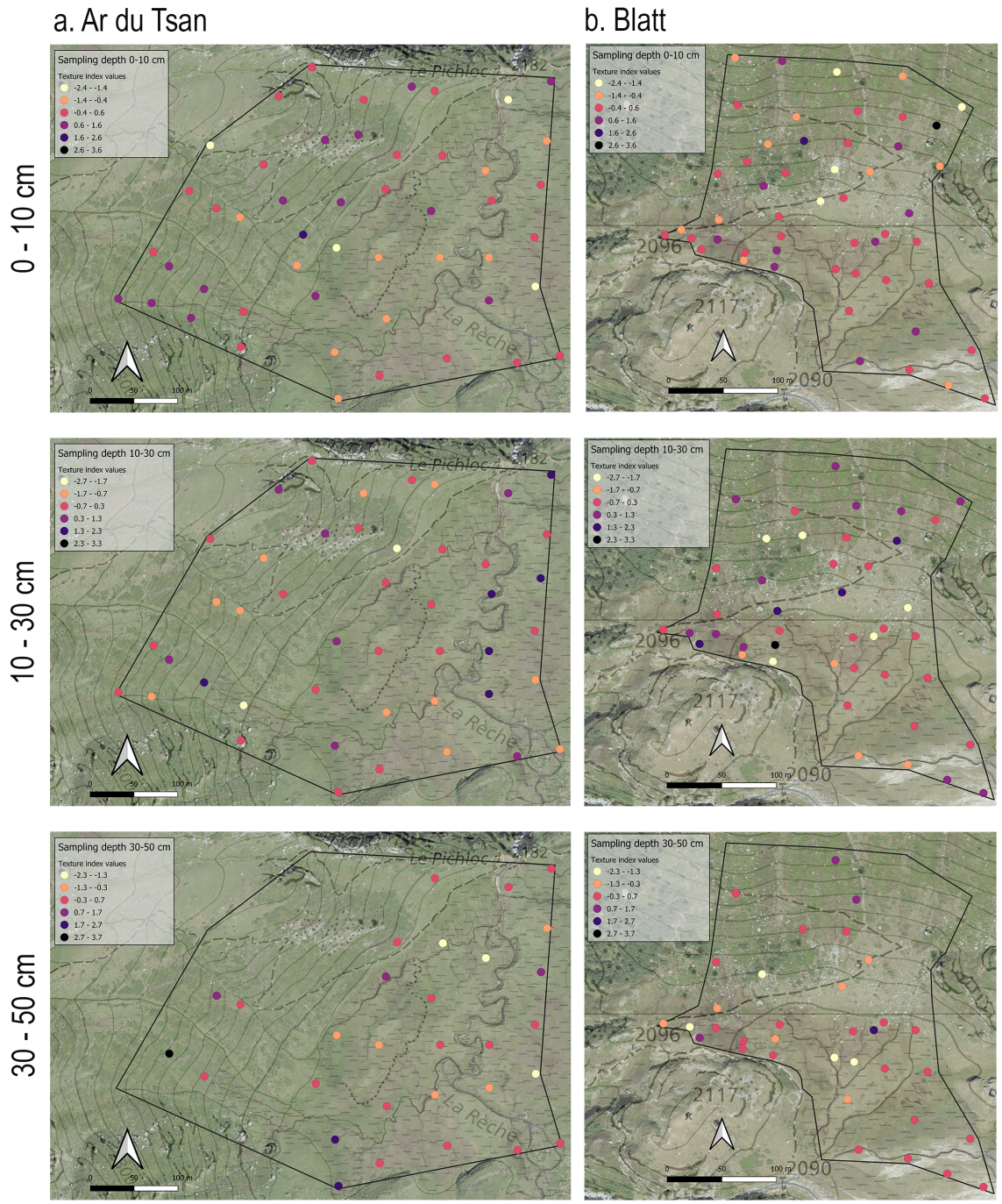

Figure S10: Map of texture index derived from the factor analysis. Left panels show the evolution of these values with depth for Ar du Tsan, when right panels show the evolution for Blatt. The base map is an orthophoto overlaid on a topographic map (1:10'000) from Swisstopo.